Functional characterization of a "plant-like" HYL1 homolog in the cnidarian *Nematostella vectensis* indicates a conserved involvement in microRNA biogenesis

Abhinandan Mani Tripathi[1,2], Yael Admoni[1,2], Arie Fridrich[1,3], Magda Lewandowska[1,3], Joachim M. Surm[1,3], Reuven Aharoni[1], Yehu Moran[1,4]

[1]Department of Ecology, Evolution and Behavior, Alexander Silberman Institute of Life Sciences, Faculty of Science, The Hebrew University of Jerusalem, Jerusalem 9190401, Israel

[2]These authors contributed equally to this work

[3]These authors contributed equally to this work

[4]Corresponding author: yehu.moran@mail.huji.ac.il

Impact statement

Presence of a functional homolog of HYL1 in *Nematostella* vectensis, a basal animal model, indicates divergent evolution of miRNA biogenesis pathway in plants and animals from an ancestral miRNA system

Abstract

While the biogenesis of microRNAs (miRNAs) in both animals and plants depends on the RNase III Dicer, its partner proteins are considered distinct for each kingdom. Nevertheless, recent discovery of homologs of Hyponastic Leaves1 (HYL1), a "plant-specific" Dicer partner, in the metazoan phylum Cnidaria, challenges the view that miRNAs evolved convergently in animals and plants. Here we show that the HYL1 homolog Hyl1-like a (Hyl1La) is crucial for development and miRNA biogenesis in the cnidarian model *Nematostella vectensis*. Inhibition of Hyl1La by morpholinos resulted in metamorphosis arrest in *Nematostella* embryos and a significant reduction in levels of most miRNAs. Further, meta-analysis of morphants of miRNA biogenesis components, like Dicer1, shows clustering of their miRNA profiles with Hyl1La morphants. Strikingly, immunoprecipitation of Hyl1La followed by quantitative PCR revealed that in contrast to the plant HYL1, Hyl1La interacts only with precursor miRNAs and not with primary miRNAs. This was complemented by an in vitro binding assay of Hyl1La to synthetic precursor miRNA. Altogether, these results suggest that the last common ancestor of animals and plants carried a HYL1 homolog that took essential part in miRNA biogenesis and indicate early emergence of the miRNA system before plants and animals separated.

Introduction

MicroRNAs (miRNAs) are 21-24 nucleotides-long small RNAs that are known to be involved in post-transcriptional gene regulation and play important roles in both plant and animal development (Alvarez-Garcia & Miska, 2005; Bråte et al., 2018; Voinnet, 2009). The miRNA is transcribed by RNA polymerase II into a long primary transcript, which is further processed into a miRNA precursor and finally chopped into ~22 nucleotide miRNA/miRNA* duplex (Bartel, 2004, 2018; Voinnet, 2009). The processing of miRNA varies between plants and animals (Moran et al., 2017). In animals, the biogenesis of miRNAs is compartmentalized as the processing occurs in both the nucleus and cytoplasm. Within the nucleus, the RNase type III Drosha and its partner Pasha (also called DGCR8) constitute a microprocessor complex (J. Han et al., 2004; Kim et al., 2009). This complex acts on primary miRNA (pri-miRNA) transcripts and processes them into precursor miRNA (pre-miRNA). The pre-miRNA is then transported by Exportin 5 into the cytoplasm where they get further processed into the mature miRNA by the RNase type III Dicer with the help of other double-stranded RNA binding proteins such as Loquacious (Loqs), Transactivation response element RNA-binding protein (TRBP) and protein activator of the interferon-induced protein kinase (PACT) (J. Han et al., 2004; Redfern et al., 2013; Saito et al., 2005). Contrastingly, in plants both pri-miRNA and pre-miRNA are processed into mature miRNA by a single RNase type III, called DICER-LIKE1 (DCL1) assisted by its partner the double-stranded RNA binding

motif (DSRM)-containing protein, Hyponastic Leaves1 (HYL1) within the nucleus (M.-H. Han et al., 2004; Voinnet, 2009). In both plants and animals, the mature miRNA duplex interacts with Argonaute proteins (AGOs) and forms the RNA-induced silencing complex (RISC) in the cytoplasm. The RISC complex commences miRNA guided cleavage or translational inhibition of complementary targets genes (Kim et al., 2009).

The metazoan lineages of Bilateria and its sister group Cnidaria separated more than 600 million years ago (MYA). While Bilateria include the vast majority of animals, Cnidaria include sea anemones, corals, hydroids and jellyfish. The phylogenetic position of cnidarians makes them an important comparative group for inferring animal evolution. In a previous study, we identified different components of miRNA biogenesis machinery in Cnidaria and observed that most bilaterian components have cnidarian homologs. However, cnidarians lack homologs of classical bilaterian Dicer protein partners such as PACT, Loqs or TRBP (Moran et al., 2013). Interestingly two homologs of HYL1 called Hyl1-Like-a (NveHyl1La) and Hyl1-Like-b (NveHyl1Lb) were identified in the sea anemone *Nematostella vectensis* (Moran et al., 2013). Apart from this, it was also found that cnidarian miRNAs possess several interesting features that are common to their counterparts in plants: cnidarian miRNAs and their targets show perfect complementarity and frequently regulate their targets by messenger RNA (mRNA) cleavage (Moran et al., 2014). Recently, some other common features with plants were identified in *Nematostella*, including methylation of miRNAs by HEN1 (Modepalli et al., 2018), a feature rarely found in animals and the origin of miRNAs from inverted duplication of their target genes (Fridrich et al., 2020), a feature previously considered specific to plant miRNAs.

In addition to the presence of HYL1 homologs in Cnidaria, homologs are also present in other non-bilaterian animals such as sponges (*Amphimedon queenslandica*) and in ctenophores (*Mnemiopsis leidyi*) (Figure 1) (Moran et al., 2013). However, we could not detect HYL1 homologs in Placozoa (*Trichoplax adhaerens*) (Figure 1A). Additionally, we also could not find any homologs in bilaterian animals and in unicellular organism like Fungi and Ichthyosporea. However, deep phylogenetic study of DSRM proteins showed that those of protozoans and fungi are phylogenetically closer to the DSRM proteins of plants (Dias et al., 2017). These results suggested that the HYL1-like proteins were already present in the common ancestor of plants and animals and during evolution have been lost in Bilateria and Ichthyosporea. These sequence-based observations led us to experimentally test the function of a HYL1 homolog of *Nematostella,* which could provide better insight into the evolution and origin of the miRNA biogenesis pathway. Our results show that Hyl1La is essential for the development of *Nematostella* and miRNA biogenesis, suggesting a common evolutionary history of miRNA biogenesis in plants and animals.

Results

Hyl1La plays an essential role in *Nematostella* development

Mutants of miRNA biogenesis pathway components exhibit severe developmental defects in both plants and animals (Alvarez-Garcia & Miska, 2005; Schauer et al., 2002). The HYL1 protein is known to play an essential role in the growth and development of the model plant *Arabidopsis thaliana* by regulating miRNA biogenesis (Achkar et al., 2018; M.-H. Han et al., 2004). Similarly, in mice, TRBP mutants show multiple developmental abnormities and a reduction in miRNA accumulation (Koscianska et al., 2011; Zhong et al., 1999). The *Hyl1La* gene of *Nematostella* contains 11 exons and 10 introns predicted to code for a protein containing three DSRM domains (Figure 1B and Figure 2A). Unlike its paralog *Hyl1Lb* that is specific to stinging cells and carries additional protein domains, *Hyl1La* expression is ubiquitously distributed throughout *Nematostella* tissues and shares its domain structure with other cnidarian HYL1 homologs (Moran et al., 2013). Thus, we decided to focus our analysis on this gene. To decipher the function of Hyl1La in *Nematostella*, we designed two different splicing morpholinos (Hyl1La SI MO1 and Hyl1La SI MO2) to knockdown by mis-splicing the gene at two different intron-exons junctions. Additionally, the gene was also targeted for inhibition by using a translation-blocking morpholino (Hyl1La TB MO) which binds on the 5′ UTR and sterically blocks translation (Figure 2A). We injected each of the three MOs into *Nematostella* zygotes in parallel with a control morpholino (Control MO) designed to bind to no target in the sea anemone genome. The effect of SI MOs was validated by PCR followed by cloning and sequencing which revealed intron retention in both cases (Figure 2-figure supplement 1-source data1 and Supplementary file 1). All the injected animals were studied until nine days post-fertilization (dpf). We observed that more than 80% of the animals injected with control MO developed normally and metamorphosed into primary polyps. In contrast, the animals injected with any of the three Hyl1La MOs showed developmental abnormalities, where more than 90% of the animals did not settle and metamorphosed into primary polyps until nine days post-fertilization (dpf) (Figure 2B-D and F). The developmental abnormalities observed here were grossly similar to those observed in *Nematostella* morphants of other miRNA processing components such as HEN1, Dicer1, AGO1 and AGO2 knockdown animals (Fridrich et al., 2020; Modepalli et al., 2018) (Figure 2E). These results indicate that Hyl1La plays an essential role in *Nematostella* development, possibly by regulating the processing and expression of miRNAs.

Hyl1La regulates the miRNA biogenesis

129 The above observed metamorphosis arrest suggested the possible involvement of Hyl1La in
130 miRNA biogenesis, as mutants defective in their miRNA biogenesis exhibit abnormal development in
131 both animals and plants (Achkar et al., 2018; Zhong et al., 1999). HYL1 in *Arabidopsis* interacts with the
132 stem region of miRNA precursors by using its DSRM domains and works with DCL1 synergistically
133 (Song et al., 2007; Wu et al., 2007). Although the Dicer homolog alone is capable of processing the
134 precursor into a mature miRNA, the presence of HYL1 is essential as it enhances the efficiency and in
135 some cases the accuracy of miRNA biogenesis in plants (Dong et al., 2008; Szarzynska et al., 2009). To
136 assay the possible role of Hyl1La on miRNA expression in *Nematostella*, we performed small RNA
137 sequencing of animals, injected with Hyl1La SI MO1 and with control MO. The analysis of read length
138 distribution showed that the small RNA reads that lied between the size of miRNAs (20-24 nt) were
139 higher ($P < 0.01$, Student's t-test) in control as compared to knockdown embryos (Figure 3A). Further, we
140 analyzed the miRNA expression by using miRProf (Stocks et al., 2012) and normalized the miRNA reads
141 in transcripts per million (TPM) (Supplementary file 2). For the miRNA quantification we used the most
142 recent *Nematostella* miRNA datasets that were obtained by AGO-immunoprecipitation (Fridrich et al.,
143 2020). The expression of normalized miRNA reads was compared between control and Hyl1La SI MO1.
144 About 54% of the total identified miRNAs showed downregulation of more than two-fold in Hyl1La SI
145 MO1 injected animals as compared to the control (Figure 3B). Further, a significant reduction in overall
146 miRNA abundance was observed in the knockdown morphants ($P < 0.00001$, Wilcoxon signed-rank test)
147 (Figure 3C). The expression variation caused by the action of other two morpholinos (Hyl1La SI MO2
148 and Hyl1La TB) was also assayed by quantitative stem-loop PCR of five miRNAs (Figure 3D and Figure
149 3-figure supplement 1). Significant downregulation of three miRNAs: miR2022-3p, miR2025-3p and
150 miR2026-5p was detected in all three MOs (with the exception of miR-2026-5p with SI MO1), which
151 supported the small RNA sequencing results. In contrast, two miRNAs, miR2027-5p and miR2028-5p
152 either showed upregulation or were not significantly affected by the Hyl1La knockdown. Previous studies
153 have also shown that these two miRNAs may respond differently to other miRNAs in HEN1 and Dicer1
154 knockdown morphants of *Nematostella* (Modepalli et al., 2018). This might be relevant to other miRNAs
155 that did not show downregulation and suggest differences in their biogenesis. Further, we also checked
156 for the processing accuracy of all the identified miRNAs by mapping them onto their respective
157 precursors. The analysis did not reveal any aberrant processing. These results suggest that like its
158 homolog in plants, Hyl1La in *Nematostella* might be involved in enhancement of Dicer efficiency and is
159 not involved in size selection.

160 To further explore the effect Hyl1La knockdown has on the expression of mature miRNAs in
161 *Nematostella*, we performed a meta-analysis comparing the effect of knocking down previously

162 characterized miRNA biogenesis components such as HEN1, Dicer1, AGO1 and AGO2 (Fridrich et al.,
163 2020; Modepalli et al., 2018) (Figure 2G and supplementary file 3). Using principal component analysis
164 (PCA), we see that broadly the expression of mature miRNAs following the knockdown of Hyl1La
165 functions similarly to other characterized miRNA processing components. This is evident with Hyl1La
166 morphants clustering with all miRNA biogenesis components compared to control, particularly with
167 HEN1 and Dicer1. We also observe that both AGO1 and AGO2 are the most distant among the miRNA
168 biogenesis components, which is consistent with their function of loading and therefore affecting a
169 particular subset of miRNAs (Fridrich et al., 2020), while Hyl1La, HEN1 and Dicer1 affect the majority
170 of the same miRNA in the same manner.

171 Next, we explored the effect of Hyl1La MO on other categories of small RNAs (siRNA and
172 piRNA) reported in *Nematostella* (Modepalli et al., 2018; Praher et al., 2017). The expression of
173 normalized reads of siRNA and piRNAs were compared between control and Hyl1La MO injected
174 animals. Significant ($P < 0.00001$, Wilcoxon signed-rank test) down- and up-regulation of siRNAs and
175 piRNAs, respectively were observed in Hyl1La MO depleted animals (Figure 3-figure supplement 2A-D).
176 In case of siRNAs the difference was very mild as only 9% (46 out of 469) of siRNAs showed
177 downregulation of more than two-fold in Hyl1La MO injected animals (Figure 3-figure supplement 2A).
178 Contrastingly, most of the piRNAs showed upregulation in Hyl1La depleted animals wherein 36% (91
179 out of 251) of piRNAs showed upregulation of more than two-fold (Figure 3-figure supplement 2C). In
180 addition, the size distribution of reads shows upregulation ($P < 0.05$, Student's t-test) of sizes that
181 correspond to piRNAs (28-30 nt) (Figure 3A). Overall small RNA analysis showed that Hyl1La depletion
182 has strong effect on miRNA expression, while mild and opposite effect on siRNA and piRNA expression,
183 respectively.

184 To further support our results obtained with MOs, we attempted to knockdown this gene by using
185 short-hairpin RNAs (shRNAs), a method previously established in *Nematostella* (Karabulut et al., 2019)
186 that worked well in our lab for other genes (Lewandowska et al., 2021). We designed three different
187 shRNAs from three different regions of Hyl1La gene (Hyl1La shRNA1, Hyl1La shRNA2 and Hyl1La
188 shRNA3) (Figure 4A-C) and injected them into *Nematostella* zygotes. In parallel we also used a control
189 shRNA with no target in *Nematostella* genome that was previously used as control for similar
190 experiments (He et al., 2018; Karabulut et al., 2019). To assess the effect of these shRNAs on Hyl1La
191 expression, we performed qRT-PCR from three days old injected animals. Unexpectedly, we did not find
192 any difference in Hyl1La expression (Figure 4D). Additionally, we also assessed the phenotype, but we
193 could not identify any phenotypic difference either. Next, we employed stem-loop PCR to test whether
194 small RNAs are generated from an injected shRNA and indeed the small RNAs were produced as

195 expected (Figure 4E). This result indicates that the small RNAs derived from the shRNAs were not able
196 to down regulate Hyl1La.

197 **Hyl1La interacts with pre-miRNAs but not with pri-miRNAs**

198 The above observed reduction in miRNA expression indicates the possible involvement of
199 Hyl1La in miRNA biogenesis. Being a DSRM containing protein, it could interact either with pri-
200 miRNA, pre-miRNA or with both. Hence to test if Hyl1La interacts with pre- and/or pri-miRNA we
201 conducted an immunoprecipitation (IP) assay by injecting a plasmid carrying a cassette encoding an N-
202 terminal 3×FLAG-tagged full-length Hyl1La ("FLAG- Hyl1La") followed by a 3′-memOrange2
203 separated by a P2A self-cleaving peptide (Figure 5A) (Kim et al., 2011; Shaner et al., 2008). The
204 expression of the FLAG-Hyl1La cassette was confirmed by visualizing the animals under fluorescence
205 microscope (Figure 5B) and by using anti-FLAG western blot (Figure 5- figure supplement 1A-source
206 data 1 and 2). Further, RNA immunoprecipitation (RIP) with anti-FLAG antibody was performed (Figure
207 5C-source data 3 and 4) in three different biological replicates followed by qPCR analysis. Interestingly,
208 we observed that there was very poor enrichment of pri-miRNA (Ct-values >30, sometimes undetected)
209 as compared to pre-miRNA (Supplementary file 4 and Figure 5- figure supplement 1 B-C-source data 5
210 and 6). Due to the very high Ct values measured for pri-miRNA we were not able to compare the levels of
211 pri-miRNAs bound with IgG and accurately compare them to FLAG-Hyl1La. Interestingly, when we
212 compared the enrichment of pre-miRNAs, we found that six out of eight were significantly enriched in
213 FLAG-Hyl1La IP in comparison to IgG, with miR-2023 showing a trend similar to other miRNAs but not
214 reaching significance (Figure 5D and Figure 5- figure supplement 1-source data 5 and 6). Expectedly,
215 miR-2029 showed no enrichment in anti-FLAG samples. This miRNA might be processed independently
216 of Hyl1La since it is also not significantly decreased following Hyl1La and Dicer1 knockdowns
217 (Modepalli et al., 2018). Taken together, these results showed that Hyl1La interacts with pre-miRNA but
218 not with pri-miRNA.

219 Next, we generated libraries from FLAG-Hyl1La immunoprecipitated samples and analyzed the
220 expression of additional longer (>100 bp) transcripts (Figure 5- figure supplement 4 and supplementary
221 file 5). We observed no significant enrichment for pri-miRNA, mRNA, non-coding RNA (rRNA,
222 snoRNA and tRNA) and repetitive elements. These results suggest that Hyl1La specifically binds pre-
223 miRNAs. To further validate Hyl1La affinity to pre-miRNAs, we tested Hyl1La binding to pre-miRNAs
224 via in vitro binding assay. We generated synthetic pre-miRNAs based on the pre-miR-2022 backbone
225 with the mature miRNA sequence changed so it will not target *Nematostella* genes. As a control we used
226 a shuffled version of the same pre-miRNA that does not create a hairpin secondary structure (Figure 6A-

227 B). Both pre-miRNAs were labeled with biotin at their 3' end and incubated with protein lysates from
228 FLAG-Hyl1La expressing animals in three biological replicates. Western blot conducted with anti-FLAG
229 antibodies revealed Hyl1La binding the pre-miRNA with significantly higher efficiency than the shuffled
230 sequence (Figure 6C-D – source data 1-6 and supplementary file 6), thus supporting the specific affinity
231 of Hyl1La to miRNA precursors.

232 **Discussion**

233 Altogether the absence of animal-like Dicer partner proteins such as TRBP or PACT and
234 presence of a functional homolog of HYL1 (Hyl1La) in *Nematostella* indicated that a Hyl1-like protein
235 might have been present in the last common ancestor of plants and animals. Apart from *Nematostella*, the
236 presence of HYL1 homologs in additional members of Cnidaria and other non-bilaterian metazoan groups
237 such as sponges (Figure 1A) further strengthens the notion of common ancestry of the miRNA systems of
238 plants and animals. Further, while the cleavage mode of action and nearly-perfect target binding could
239 have evolved convergently in plants and cnidarians (Moran et al., 2014), the involvement in miRNA
240 biogenesis of the Hyl1L in Cnidaria and its plant homolog HYL1 is far less likely to be the result of
241 parallel evolution. This is because the former might be driven by functional constraints or advantage in
242 cleaving miRNA targets whereas the latter would require the independent recruitment of the same protein
243 into the same system. Thus, our results call into question the hypothesis that miRNAs evolved
244 convergently in plants and animals from an ancestral RNAi system (Axtell et al., 2011; Tarver et al.,
245 2012). To the best of our knowledge, our study provides the first demonstration that an elaborate miRNA
246 biogenesis pathway might have existed in the common ancestor of plants and animals. However, it is also
247 important to note that the presence of HYL1-like proteins by itself cannot be considered a definitive
248 hallmark for the existence of miRNAs in non-bilaterian animals or their relatives. For example, a
249 homolog of HYL1 exists in the ctenophore *M. leidyi*, but this species does not produce miRNAs (Figure
250 1A) (Maxwell et al., 2012). Moreover, several unicellular relatives of animals contain miRNAs, but no
251 homologs of HYL1 (Bråte et al., 2018). Thus, this pathway might demonstrate in various lineages
252 compositional flexibility as well as high loss rates (Reviewed in (Moran et al., 2017). Recently, it was
253 found in *Chlamydomonas* (a unicellular green algae) that DUS16, which is a DSRM protein, and the
254 RNase III DCL3 were efficient enough for miRNA processing (Yamasaki et al., 2016). Further, various
255 fungal groups also exhibit the presence of Dicer and plant-like DSRM proteins and lack animal-like
256 accessory proteins, such as Drosha and Pasha (Dang et al., 2011; Dias et al., 2017). Contrastingly, DCL3
257 of *Chlamydomonas* exhibits some structural features that are reminiscent of metazoan Drosha (Valli et al.,
258 2016). These observations suggest that the common ancestor of all these groups might have harbored only

259 a single Dicer/Drosha-like RNase III enzyme assisted by a DSRM protein resembling the ones found in
260 plants (HYL1-like).

261 We unexpectedly found that in contrast to plant HYL1 proteins, which interacts with both pri-
262 and pre-miRNA, Hyl1La in *Nematostella* interacts only with pre-miRNA and not with pri-miRNA
263 (Figure 5D). Our sequencing data strengthens the specificity of the pre-miRNA binding by showing no
264 enrichment for additional longer RNA molecules (Figure 5- figure supplement 4A). Further supporting
265 the specific binding of Hyl1La to pre-miRNAs is the in vitro binding assay to a synthetic pre-miRNA
266 compared to the shuffled sequence with a different secondary structure (Figure 6D). A plausible
267 explanation to this finding might be that *Nematostella* already possesses miRNA biogenesis machinery
268 like the Drosha-Pasha microprocessor (Moran et al., 2013) that is known to interact only with pri-
269 miRNAs and crop them into the pre-miRNAs (Kim et al., 2009). Another surprising finding in this study
270 is that we were able to knockdown the Hyl1La by using the morpholino only and not by shRNA
271 microinjection, despite the processing of the shRNA (Figure 4D-E). A possible explanation for this
272 contrasting result between MO and shRNA probably lies between the different mode of action of these
273 two molecules. In contrast to MOs that do not use the cellular machinery, shRNA requires the
274 miRNA/RNAi machinery for their production as well as in target recognition and inhibition. Thus, our
275 combined results suggest that Hyl1La might have an additional effect on biogenesis steps that are
276 downstream to the cleavage by Dicer such as loading of small RNAs into AGO, the protein at the heart of
277 the RNA-induced silencing complex (RISC) (Hutvagner & Simard, 2008). Under such a condition the
278 shRNA-derived small RNA would be unable to load onto RISC and hence could not cleave the Hyl1La,
279 rendering its expression unaffected. Further, in such a scenario after injection with the shRNAs the
280 system might reach a balance point that is very close to the normal Hyl1La levels. Alternatively, it is
281 possible that the three shRNAs are ineffective due to lack of accessibility of the three distinct target sites
282 on the Hyl1La transcript to the RISC loaded with the shRNA derived small RNAs for reasons such as
283 secondary structure or binding by other proteins that restrict the RISC accessibility. However, we find this
284 explanation less likely because the three shRNAs target distinct parts of this relatively long transcript.

285 During small RNA analysis, we expectedly observed a strong reduction in miRNA expression but
286 in parallel a mild reduction in siRNA expression was also observed in Hyl1La-depleted animals (Figure 3
287 and Figure 3- figure supplement 2A-B). This might be due to involvement of Hyl1La in siRNA
288 biogenesis pathway in *Nematostella*. Similar observation was also reported in *Arabidopsis* where different
289 members of the DRB protein family, which includes HYL1, are known to be involved in biogenesis of
290 different siRNAs and hinder their expression (Curtin et al., 2008; Raja et al., 2014). For example, a HYL1
291 (DRB1) mutant of *Arabidopsis* exhibits severe defects in miRNA expression but also has a partial effect

292 on tasiRNA (a plant-specific category of siRNAs) expression (Tagami et al., 2009). Further, DRB2 and
293 DRB4 were shown to inhibit small RNA expression produced by RNA polymerase IV (Pélissier et al.,
294 2011). In addition to miRNAs and siRNAs an opposite trend in piRNA expression was also observed as
295 most of the piRNAs were up-regulated in Hyl1La-depleted animals (Figure 3A and Figure 3- figure
296 supplement 2C-D). We propose this might be due to the fact that depletion of Hyl1La-dependent miRNAs
297 provided a void in the sequencing libraries that in turn made more reads available for piRNAs.

298 Finally, here we report that Hyl1La plays an important role in miRNA biogenesis in
299 *Nematostella*, a representative of Cnidaria which is the sister group of Bilateria. However, the functional
300 importance of Hyl1La in *Nematostella* identified here raises another interesting evolutionary question of
301 what led to the replacement of Hyl1La by other DSRM proteins like TRBP, Loqs or PACT in bilaterian
302 animals during evolution (Figure 1A). Interestingly, both Loqs in flies and TRBP in mammals, enable
303 processing of some miRNA precursors into different mature miRNAs and by this significantly increase
304 their variability and targeted sequences (Fukunaga et al., 2012; Lee & Doudna, 2012). Such variability is
305 currently unknown in plants or cnidarians. It is intriguing to consider the possibility that this ability of the
306 bilaterian proteins to increase small RNA variability was advantageous over Hyl1-like proteins and led to
307 the loss of the latter in bilaterian lineages.
308

309 **MATERIALS AND METHODS**

310 **Key resources table**

Reagent type (species) or resource	**Designation**	**Source or reference**	**Identifiers**
Escherichia coli	Strain DH5α	New England Biolabs	NEB-C2987I
Chemical compound	Trizol	Thermo (Ambion)	15596026
Chemical compound	Tryptone	Merck Millipore	61930505001730
Chemical compound	Yeast extract purified for Microbiology	Merck Millipore	61931105001730
Chemical compound	Agar purified for Microbiology	Merck Millipore	61939005001730

Chemical compound, drug	Ampicillin	ROTH	K029.1
Chemical compound	Dextran Alexa Fluor 488	Thermo (Molecular Probes)	D22910
Chemical compound	Red sea salt	Red sea	
Chemical compound	L-Cysteine	Merck Millipore	1028380100
Commercial Assay or kit	SuperScript III Reverse Transcriptase	Thermo (Invitrogen)	18080044
Commercial Assay or kit	Fast SYBR® Green Master Mix	Thermo (ABI)	AB-4385612
Commercial Assay or kit	Q5® High-Fidelity DNA Polymerase	New England Biolabs	NEB-M0493S
Commercial Assay or kit	AmpliScribe™ T7-Flash™ Transcription Kit	Lucigen	ASF3507
Commercial Assay or kit	Quick-RNA Miniprep	Zymo Research	R1054
Commercial Assay or kit	NucleoSpin Gel and PCR Clean-up	Macherey-Nagel	MAN-740609.50
Commercial Assay or kit	CloneJet cloning kit	Thermo (Fermentas)	K1231
Commercial Assay or kit	NextSeq 500/550 v2 Kits (75 cycles)	Illumina	FC-404-2005
Commercial Assay or kit	NEBNext Multiplex Small RNA Library Prep Set for Illumina (1-12) - 24 rxns	New England Biolabs	NEB-E7300S
Commercial Assay or kit	Pierce RNA 3' End Biotinylation Kit	Thermo Fisher Scientific	20160
Commercial Assay or kit	Ovation® SoLo RNA-seq systems kit	Tecan Genomics	0500-32
Nematostella	Lab strain, Rhode River, MD	Lab strain	

vectensis			
Software, algorithm	miRDeep2	doi:10.1093/nar/gkr688 (2012)	
Software, algorithm	The UEA small RNA Workbench	doi: 10.1093/bioinformatics/bts311	
Software, algorithm	Trimmomatic (v3.4)	doi: 10.1093/bioinformatics/btu170. Epub 2014 Apr 1	
Software, algorithm	STAR (v2.7.9)	doi.org/10.1093/bioinformatics/bts635	
Software, algorithm	RSEM	doi.org/10.1186/1471-2105-12-323	
Software, algorithm	shRNA design	doi.org/10.1016/j.ydbio.2019.01.005	www.invivogen.com/sirnawizard/index
Software, algorithm	Protein Domain Search	pfam.xfam.org/search#tabview=t	
Software, algorithm	Homologs search	blast.ncbi.nlm.nih.gov/Blast.cgi/Proteins	
Oligonucleotides	PCR Primers	Integrated DNA Technologies	In this paper
Oligonucleotides	DNA template of shRNA	Integrated DNA Technologies	In this paper
modified oligonucleotides	Morpholino	Gene Tools	In this paper
Antibody	Monoclonal mouse anti-FLAG M2 antibody	Sigma-Aldrich	F1804-50UG
Antibody	Total mouse IgG	Sigma-Aldrich	I5381-1MG

311

312 **Animal culture and microinjection**

313 *Nematostella* were grown in 16‰ artificial salt water (ASW) at 18 °C in a dark culture room. The
314 growing animals were fed with freshly hatched *Artemia salina* nauplii three times a week. Induction of
315 spawning was performed as previously described (Genikhovich & Technau, 2009): the mature male and
316 female animals were induced to produce eggs and sperm by placing them in an incubator for eight hours
317 under constant white light and heat (25 °C). After induction, the tanks were further kept at 18 °C (in the
318 culture room) for two hours to allow the release of egg packages and sperm. Further, the egg packages
319 were fertilized for 30 min by placing the packages inside the male tanks. The quality of egg packages was
320 checked under the stereomicroscope and egg packages of round shape and homogenous size were
321 processed further for dejellying using 3% of L-Cysteine in 16‰ ASW pH 7.2 (titrated with 10 M NaOH).
322 The selected egg packages were kept in the cysteine solution for 15 min while rotated by hand. The eggs
323 were washed using 16‰ ASW in tissue culture plates. These clean eggs (zygotes) were further used for
324 microinjection. For microinjection 1 mM stock solutions of both morpholino and shRNA were prepared
325 by dissolving them into nuclease-free water. The toxicity of morpholinos as well as shRNA was
326 optimized by injecting different concentrations into the animals along with the control injected animals.
327 Concentrations resulting in toxicity of less than 30% of the animals (estimated morphologically in the two
328 days following the injection) were considered suitable for injection. All morpholinos used in this study
329 were designed and synthesized by Gene Tools, LLC (USA). The same control morpholino was used in all
330 experiments.

331 Hyl1La TB MO (Translation Blocking) GGCCGCCATTTCTTAGAGAAGTTCA

332 Hyl1La SI MO1 (Splicing inhibition) AGAAACAGACTTGTACCTTTTTGTA

333 Hyl1La SI MO2 (Splicing inhibition) CTTGTTGTAGTCTAAGCCTTACCAT

334 Dicer1 TB MO (Translation Blocking) ATTCCTCTTCGTCACTTGACATCTT

335 Control MO (Standard control MO) CCTCTTACCTCAGTTACAATTTATA

336 We found that the optimum concentrations were 300 µM, 900 µM and 450 µM for the Hyl1La
337 TB, Hyl1La SI MO1 and Hyl1La SI MO2, respectively. Dicer1 TB MO was injected at the concentration
338 of 805 µM. For all the three shRNAs, 600 ng/µl concertation was found to be suitable. Similar
339 concentration of control MO was used for microinjection in parallel with Hyl1La MOs. In every shift, we
340 injected 600 zygotes (300 Control MO and 300 Hyl1La MO) by mixing the injected material with dextran
341 Alexa Fluor 488 (Thermo Fisher Scientific, USA) which was used as a fluorescent tracer while injection
342 was carried under magnification by a TS-100F fluorescent microscope (Nikon, Japan). The injected
343 zygotes were kept at 22 °C for further growth. The morphology of the animals was observed for up to

344 nine days after which the number of settled and unsettled animals were counted and documented under
345 SMZ-18 fluorescent stereomicroscope (Nikon). Animals injected with Dicer1 MO were observed and
346 documented after ten days. For RNA extraction microinjected zygotes were flash frozen in liquid nitrogen
347 after three days of growth and stored at -80 °C until RNA extraction. All the MO and shRNA injection
348 experiments were performed in three independent biological replicates with three distinct animals'
349 batches. Dicer1 MO injection was performed in one replicate to repeat an experiment with published
350 results (Modepalli et al., 2018).

351 **Small RNA sequencing and analysis**

352 The RNA was isolated using Trizol (Thermo Fisher Scientific) from three days old animals.
353 Small RNA sequencing was performed for only Hyl1La SI MO1 and control MO injected animals. The
354 small RNA library was prepared using NEBNext Multiplex Small RNA Library Prep Illumina kit (New
355 England Biolabs, USA) with some modifications (Plotnikova et al., 2019). In brief, small RNAs were
356 isolated (18nt-30nt) from 1 µg of total RNA using 15% urea-PAGE (Bio-Rad, USA) followed by
357 overnight precipitation using 0.3% NaCl. The size-selected small RNAs were further precipitated using
358 ice-cold ethanol (2.5× volume) and 1 µl of GlycoBlue (Thermo Fisher Scientific) by centrifugation at
359 21130 × *g*. The pellet was dissolved in 7.5 µl nuclease-free water and used further for adapter ligation.
360 The ligated products were subjected to 14 cycles of PCR amplification using adapter specific primers.
361 The PCR product was run on 2% agarose gel followed by staining with GelRed (Biotium, USA). The
362 band size between 137nt–149nt was selected and purified using Gel Extraction Kit (Macherey-Nagel,
363 Germany). The quality of the purified product (sRNA-seq libraries) was checked by using TapeStation
364 system (Agilent, USA). The libraries having a dominant peak at the size range of 137nt–149nt were
365 sequenced by NextSeq500 (Illumina) in single-end mode.

366 The small RNA data was analyzed using miRProf (Stocks et al., 2012) with the following
367 parameters: two mismatches allowed, minimum abundance of 1 for miRNA and 5 for piRNA and siRNA,
368 allowed overhang and not grouping mature and star strands. For miRNA, piRNA and siRNA analysis we
369 mapped the small RNA sequences after adapter removal on the relevant previously reported sets of
370 *Nematostella* small RNAs (Fridrich et al., 2020; Modepalli et al., 2018; Praher et al., 2017). The small
371 RNA expression was normalized in TPM (transcripts per million) by using only the transcripts that
372 mapped on the reference genome. For read length distribution and scattered plot we used the average of
373 expression obtained from the three biological replicates. For mapping onto the genome and miRNA
374 precursor for identification of aberrant processing of miRNA, miRDeep2 (Friedländer et al., 2012) was
375 used.

376 Meta-analysis was performed to compare the pattern of miRNA expression following the
377 knockdown of miRNA biogenesis components. Raw reads from small RNA-seq experiments involving
378 the knockdown of various miRNA biogenesis components (Hyl1La, Dicer1, HEN1, AGO1 and AGO2)
379 were downloaded from the NCBI Sequence Read Archive (Fridrich et al., 2020; Modepalli et al., 2018).
380 Raw reads were trimmed using Cutadapt (v3.4)(Martin, 2011) and sequences shorter than 18 nt were
381 discarded. Filtered reads were mapped to the *Nematostella* genome using Bowtie (v1.3.1)(Langmead et
382 al., 2009) and miRNA loci quantified using featureCounts (v2.0.0)(Liao et al., 2014) from previously
383 characterized coordinates. Due to differences in developmental stages and library preparation, reads were
384 normalized between morphants and their respective control samples. Principle component analysis was
385 then performed using these normalized values using ggplot2 in R (v4.1.0).

386 **Total RNA sequencing and analysis**

387 To generate total RNA libraries from immunoprecipitated samples, RNA was extracted with 1 ml
388 Trizol (Thermo Fisher Scientific) and purified following the manufacturer's protocol. To increase the
389 yield, we added 1 µl of RNA-grade glycogen (Roche, Switzerland) into the isopropanol during the
390 precipitation step and conducted two rounds of 75% ice-cold ethanol washes. RNA pellets were dissolved
391 with 8 µl low-EDTA TE buffer (Thermo Fisher Scientific) and diluted with 0.1% Tween-20 (Sigma-
392 Aldrich, USA). The samples were prepared for sequencing using Ovation® SoLo RNA-seq systems kit
393 (Tecan Genomics, USA) according to the manufacturer's protocol with the exclusion of the AnyDeplete
394 stage. The samples were amplified for 13, 14 and 16 cycles using uniquely barcoded adaptors provided in
395 the kit. The quality and size distribution of the produced libraries was checked using TapeStation system
396 (Agilent, USA). The pooled libraries were run on NextSeq500 (Illumina) in the concentration of 1.1 pM.

397 Raw reads were processed by Trimmomatic (v3.4), using the following parameters
398 (HEADCROP:9 LEADING:3 TRAILING:3 SLIDINGWINDOW:4:20 MINLEN:36) (Bolger et al.,
399 2014). High-quality reads retained were mapped to the *Nematostella* genome (JGI.Nemve1) using STAR
400 (v2.7.9) (Dobin et al., 2013) and de-duplexed using NuDup (nugentechnologies.github.io/nudup/).
401 Transcript abundances were estimated to previously characterized coding (Schwaiger et al., 2014) and
402 noncoding RNA (Fridrich et al., 2020; Modepalli et al., 2018) using RSEM (v1.3) (Li & Dewey, 2011)
403 and cross-sample normalized using TMM (Robinson & Oshlack, 2010).

404 **Synthesis of shRNA**

405 Potential shRNA precursors for Hyl1La gene were predicted using the shRNA prediction tools
406 (https://www.invivogen.com/sirnawizard/index.php) (Karabulut et al., 2019). Three precursors from three

407 different regions were further chosen, all having GC content of more than 35%. Further, we also added to
408 the sequence a T7 promotor and three different mismatches at nucleotide positions 10, 13 and 16 to create
409 bulges in the precursors (Figure 4A-C). All these modified precursors were reverse complemented and
410 synthesized at the DNA level by Integrated DNA Technologies, Inc. (IDT, USA). The DNA templates
411 and reverse primer were mixed (1:1) and denatured at 98 °C for 5 min and cooled to 24 °C. Further, this
412 mixture was mixed with the components of AmpliScribe™ T7-Flash™ Transcription Kit (Lucigen, USA)
413 and incubated for eight hours at room temperature. The in vitro transcribed product was further purified
414 using Quick-RNA Miniprep (Zymo Research, USA). The quality and size of the precursor was checked
415 on agarose gel and its concentration was measured using Qubit RNA BR (Broad Range) Assay Kit with
416 the Qubit Fluorometer (Thermo Fisher Scientific). The concentration ranged from 1500 ng/µl to 2000
417 ng/µl.

418 **Reverse transcription-quantitative PCR**

419 For the quantification of Hyl1La transcripts from shRNA injected animals and for checking the
420 splicing inhibition (Hyl1La SI MO injected animals), cDNA was prepared from 500 ng of total RNA
421 using the iScript™ cDNA Synthesis Kit (Bio-Rad). For the quantification of miRNAs and shRNA, we
422 designed the stem-loop primers for five different miRNAs and shRNA (Chen et al., 2005). For cDNA
423 preparation, 100 ng of total RNA was reverse transcribed using the SuperScript™ III Reverse
424 Transcriptase (Thermo Fisher Scientific). The specificity of the miRNA primers was determined by using
425 end point PCR (Varkonyi-Gasic et al., 2007). For this, we used 2 µl of cDNA as template, miRNAs
426 specific forward primer and stem-loop specific reverse primer and run the PCR at 94 °C for 2 min,
427 followed by 35 cycles of 94 °C for 15 s and 60 °C for 1 min. For analyzing differential expression, we ran
428 qRT-PCR with 5sRNA as an internal control. For amplification of pre-miR-2029, pre-miR-2030 ad pre-
429 miR-2035-1 we used 1.5 µl of cDNA. For all the real time experiments, we used Fast SYBR® Green
430 Master Mix (Thermo Fisher Scientific) and samples were run on StepOnePlus Real-Time PCR System
431 (Thermo Fisher Scientific). All the real time experiments were performed in three independent biological
432 replicates and two technical replicates and data was analyzed using $2^{-\Delta\Delta Ct}$ method (Livak & Schmittgen,
433 2001). All the primers are listed in Supplementary file7.

434 **Cloning and sequencing of Hyl1La SI MO injected animals**

435 To validate the effect of splicing morpholinos, we designed the primers pairs spanning the introns
436 lying on the boundary of exons. PCR of the Hyl1La was done using Q5® High-Fidelity DNA Polymerase
437 (New England Biolabs). The PCR products were run on the gel and the expected-sized PCR product was
438 purified with a kit. Then the purified PCR products were ligated into the pJet2.1 vector (Thermo Fisher

439 Scientific) and transformed into the *E. coli* DH5α strain (NEB5α, New England Biolabs). The plasmids
440 were purified by a PureLink miniprep kit (Thermo Fisher Scientific) and outsourced for Sanger
441 sequencing (HyLabs, Israel).

442 **Plasmid generation**

443 Two gBlock synthetic DNA fragments (Integrated DNA Technologies) at the lengths of 1.6 kb
444 and 1.7 kb corresponding to Hyl1La fragments with a 3×FLAG tag and 20 bp overlaps were ordered used
445 for generating the expression cassette. These fragments were PCR-amplified by Q5® Hot Start High-
446 Fidelity DNA Polymerase (New England Biolabs), visualized on 1% agarose gel and purified by
447 NucleoSpin Gel and PCR Clean-up (Macherey-Nagel). Gibson assembly was performed with the
448 NEBuilder HiFi DNA Assembly Master Mix (New England Biolabs) following the manufacturer's
449 protocol. The resulting product was further subcloned by restriction digestion with *Asc*I and *Sal*I into a
450 pER242 vector having a TBP promoter previously proved to drive ubiquitous expression in *Nematostella*
451 (Admoni et al., 2020), memOrange2, and SV40 polyadenylation signal (Figure 5A). The transformation
452 was performed in *E. coli* DH5α strain (New England Biolabs). The plasmid was purified by HiSpeed
453 Plasmid Midi Kit (Qiagen, Germany) and sequenced by the Sanger method (HyLabs, Israel). 100 ng/µl of
454 purified plasmid was injected into the fertilized *Nematostella* embryo and visualized after two days under
455 an SMZ18 stereomicroscope equipped with a DS-Qi2 camera (Nikon, Japan).

456 **Hyl1La immunoprecipitation**

457 100 µl of protein G SureBeads™ magnetic beads (Bio-Rad, USA) were washed five times with
458 1× PBS (Phosphate-buffered saline). 5 µg of monoclonal mouse anti-FLAG M2 antibody (Sigma-Aldrich,
459 USA) or total mouse IgG (Sigma-Aldrich) were added to the washed beads and incubated overnight at
460 4°C on a rotating shaker. Three thousand zygotes were injected with the plasmid containing 3×FLAG-
461 Hyl1La among which ~ 2000 animals survived after two days and were used for protein extraction.
462 Protein was extracted in lysis buffer with the following composition: 25 mM Tris-HCl (pH 7.4), 150 mM
463 KCl, 25 mM EDTA, 0.5% NP-40, 1 mM DTT, Protease inhibitor cOmplete ULTRA tablets (Roche,
464 Germany) and Protease Inhibitor Cocktail Set III, EDTA-Free (Merck Millipore, USA). Murine RNase
465 inhibitor (New England Biolabs) was used in RNA processing buffer. The RNase and protease inhibitors
466 were added fresh just before use. For protein extraction, the frozen animals were mechanically
467 homogenized in 1 ml lysis buffer and incubated for rotation at 4 °C. After two hours the samples were
468 centrifuged at 16000 × *g* for 15 min at 4 ºC and supernatant was collected. Then, 100 µl of protein G
469 magnetic beads were washed thrice with 1 ml 1×PBS, once with lysis buffer and then mixed with the
470 protein lysate. The tube volume was maintained to 1.2 ml using the lysis buffer containing RNase

471 inhibitor and incubated at 4 °C on a rotating shaker (Intelli-Mixer™ ELMI, USA), for one hour. After one
472 hour, the pre-cleared lysate was collected and added to the antibody-bound beads that were preincubated
473 with the antibody overnight. These samples were incubated for two hours in rotation at 4 ºC. After
474 incubation, the beads were collected by using a magnetic stand and washed six times with lysis buffer
475 containing RNase inhibitor and one time with PBS with RNAse inhibitor. For Western blot 40 µl SDS
476 sample buffer (New England Biolabs) were added to the beads and heated at 100 °C for 8 min and placed
477 on ice for 1 min. The samples were then centrifuged for 1 min at 16,000 × *g* at 4 °C, and the supernatant
478 was collected.

479 For RNA extraction, the beads were mixed with 1 ml Trizol (Thermo Fisher Scientific) and
480 purified following the manufacturer's protocol. We added 1 µl of RNA-grade glycogen (Roche,
481 Switzerland) into the isopropanol during the precipitation step. The isolated RNA was treated with Turbo
482 DNAse (Thermo Fisher Scientific) for 30 min at 37 °C, purified with RNA Clean & Concentrator-5 kit
483 (Zymo Research), eluted in 8 µl and used for cDNA preparation.

484 **Primer designing for pre- and pri-miRNA quantification**

485 The pre-miRNA primer pairs were designed from stable stem region of precursors (Figure 5 -
486 figure supplement 2) as described previously (Schmittgen et al., 2008). The pre-miRNA sequence was
487 obtained from our recently published data (Fridrich et al., 2020). The primer pairs for pri-miRNA were
488 designed so they will anneal at least 10 nucleotides away from the pre-miRNA primers (Figure 5 - figure
489 supplement 3). These probable pri-miRNA sequences flanking the pre-miRNA were obtained from the
490 *Nematostella* genome browser (https://simrbase.stowers.org/).

491 **Biotin-labeled synthetic pre-miRNA generation**

492 Synthetic pre-miRNA for in vitro binding assay was designed based on miR-2022 backbone, with
493 the mature and star stands changed to target an mCherry synthetic gene, which is not found in the
494 *Nematostella* genome. To generate a control sequence, the original sequence was shuffled and non-
495 hairpin secondary structure was validated with RNAfold web server (Lorenz et al., 2011). The reverse
496 complement DNA templates were ordered from Integrated DNA Technologies (USA) and transcribed
497 using the AmpliScribe™ T7-Flash™ Transcription kit protocol (Lucigen). The DNase treated products
498 were cleaned with Quick-RNA MiniPrep Kit (Zymo Research), then validated on agarose gel and
499 concentration was measured with Epoch Microplate Spectrophotometer (BioTek Instruments, Inc., USA).
500 Next, 790 ng of the products were biotinylated with Pierce RNA 3' End Biotinylation Kit (Thermo Fisher
501 Scientific). After ligation of 15 h, products were cleaned according to the manufacturer's protocol and

502 pellets were dissolved with 12.5 µl nuclease-free water. A second cleaning step was conducted with
503 Quick-RNA MiniPrep Kit (Zymo Research). Products were eluted with 16 µl nuclease-free water and
504 concentration was measured with NanoDrop (Thermo Fisher Scientific).

505 **In vitro binding assay**

506 In vitro binding assay was performed according to a previously described method (Lewandowska
507 et al., 2021). In brief, 4000 zygotes were injected with the plasmid containing 3×FLAG-Hyl1La, from
508 which ~3000 survived after two days. Embryos were flash frozen with liquid nitrogen and stored in -80
509 °C. Next, animals were mechanically homogenized in the following lysis buffer: 50 mM Tris-HCl (pH
510 7.4), 150 mM KCl, 0.5% NP-40, 10% glycerol, Protease inhibitor cOmplete ULTRA tablets (Roche,
511 Switzerland), Protease Inhibitor Cocktail Set III, EDTA-Free (Merck Millipore) and Murine RNase
512 inhibitor (New England Biolabs). Protease and RNase inhibitors were added fresh just before use. Lysed
513 animals were incubated and supernatants were collected as described before. Next, the lysate was pre-
514 cleared as follows: 100 µl of streptavidin magnetic beads (New England Biolabs) were washed in 1 ml of
515 1×PBS for 3 times and the FLAG-tagged Hyl1La lysate was added to the washed beads. Lysis buffer was
516 added to make up 1.3 ml and samples were incubated at 4 °C rotation for one hour. After the incubation,
517 the pre-cleared lysates were collected and mixed with the biotin labeled pre-miRNA or biotin labeled
518 shuffled pre-miRNA as negative control in the final concentration of 8.23 ng/ml and ATP (New England
519 Biolabs) in the final concentration of 0.5 mM. Samples were incubated for one hour in rotation at room
520 temperature. Simultaneously, 100 µl of fresh streptavidin magnetic beads were washed as described
521 before and blocked with three days old wild-type lysate for one hour at 4 °C. Biotin labeled precursors
522 containing lysates were added to the blocked beads and incubated for two hours in rotation at 4 °C for
523 biotin labeled pre-miRNA pull-down. 60 µl was taken from each lysate before addition to the beads as
524 input sample. After the incubation, the lysates were discarded and the beads were washed 3 times with
525 500 µl of the following wash buffer: 50 mM Tris-HCl (pH 7.4), Protease inhibitor cOmplete ULTRA
526 tablets, Protease Inhibitor Cocktail Set III, EDTA-Free and Murine RNase inhibitor. Subsequently, 40 µl
527 of filtered double-distilled water and 20 or 30 µl of Blue Protein Loading Dye (New England Biolabs)
528 were added to the beads or the inputs, respectively. The samples were heated and centrifuged as described
529 before and the supernatant was collected for Western blot. Intensities of Western bands were determined
530 by using the ImageStudio software (Licore, UK). Enrichment of pre-miRNA pull-down compared to
531 shuffled pre-miRNA pull-down was determined by the ratio of the band to the background intensity.

532 **Quantification and statistical analysis**

533 For phenotypic analysis, we performed Student's t-test between the number of developed and
534 undeveloped animals. To test differences in size distribution of small RNA sequencing reads, Student's t-
535 test (paired two-tailed) was performed between control and Hyl1La SI MO1 samples. For statistical
536 analysis of qRT-PCR data, Student's t-test (one-tailed assuming equal variance) was performed on ΔCt
537 values between different biological replicates. For in vitro binding assay analysis, Student's t-test (paired
538 two-tailed) was performed on the ratio of the bands to background intensity. To check overall significant
539 difference between the miRNA expression levels, Wilcoxon signed-rank test was done. The Student's t-
540 test was conducted in Microsoft Excel while Wilcoxon signed-rank test was done using socscistatistics
541 (https://www.socscistatistics.com/tests/signedranks/default.aspx).

542 **Acknowledgments**

543 The authors would like to thank Dr. Michal Bronstein and Mrs. Adi Turjeman of the Centre for Genomic
544 Technologies (The Hebrew University) for their help with sequencing. This work was supported by
545 European Research Council Starting Grant 637456 CNIDARIAMICRORNA and European Research
546 Council Consolidator Grant 863809 AntiViralEvo to YM.

547 **Author contributions**

548 Conceptualization: A.M.T. and Y.M.; Methodology: A.M.T., Y.A. and Y.M.; Validation: A.M.T.;
549 Software: A.M.T. and A.F.; Formal Analysis: A.M.T., Y.A., J.M.S, A.F. and M.L.; Investigation: A.M.T.,
550 Y.A., A.F. M.L., J.M.S. and R.A.; Resources: Y.M.; Data Curation: A.M.T., Y.A. and J.M.S. ; Writing –
551 Original Draft: A.M.T., Y.A., and Y.M.; Writing –Review & Editing: A.F., M.L., J.M.S. and R.A.;
552 Visualization: A.M.T., Y.A., A.F. and J.M.S.; Supervision: Y.M.; Project Administration: Y.M.; Funding
553 Acquisition: Y.M.

554 **Additional files**

555 **Supplementary file 1** - The MO clones that are showing the intron retention.

556 **Supplementary file 2** - miRNAs and their expression.

557 **Supplementary file 3** - miRNAs and their expression for meta-analysis.

558 **Supplementary file 4** - pre-miRNA and pri-miRNA Ct values.

559 **Supplementary file 5** - RNA-seq.

560 **Supplementary file 6** - In vitro binding assay band intensities.

561 **Supplementary file 7** - Primers used in this study.

562 **Source data legends**

563 **Figure 2 - Source data1 - Related to Figure 2 - Figure supplement 1 -** This data includes the gel image
564 of aberrant Hyl1La splicing after different morpholinos injections.

565 **Figure 5 - Source data 1 - Related to Figure 5 - Figure supplement 1A -** Western blot of FLAG-
566 Hyl1La with anti-FLAG antibody.

567 **Figure 5 - Source data 2 - Related to Figure 5 - Figure supplement 1A -** Figure includes the image of
568 Western Blot Protein Ladder used as a size ruler.

569 **Figure 5 - Source data 3 - Related to Figure 5C -** Western blot of FLAG-Hyl1La after
570 immunoprecipitation.

571 **Figure 5 - Source data 4 - Related to Figure 5C -** Figure includes the image of Western Blot Protein
572 Ladder used as a size ruler.

573 **Figure 5 - Source data 5 - Related to Figure 5 - Figure supplement 1B -** Gel image of PCR amplified
574 pri-miRNA.

575 **Figure 5 - Source data 6 - Related to Figure 5 - Figure supplement 1C -** Gel image of PCR amplified
576 pre-miRNA.

577 **Figure 6 - Source data 1 - Related to Figure 6C -** Western blot of biotin pull-down with anti-FLAG
578 antibody – replicate1.

579 **Figure 6 - Source data 2 - Related to Figure 6C -** Figure includes the image of Western Blot Protein
580 Ladder used as a size ruler – replicate1.

581 **Figure 6 - Source data 3 - Related to Figure 6C -** Western blot of biotin pull-down with anti-FLAG
582 antibody – replicate2.

583 **Figure 6 - Source data 4 - Related to Figure 6C -** Figure includes the image of Western Blot Protein
584 Ladder used as a size ruler – replicate2.

585 **Figure 6 - Source data 5 - Related to Figure 6C -** Western blot of biotin pull-down with anti-FLAG
586 antibody – replicate3.

587 **Figure 6 - Source data 6 - Related to Figure 6C -** Figure includes the image of Western Blot Protein
588 Ladder used as a size ruler – replicate3.

589

590 **Data availability**

591 The RNA sequencing data were submitted to NCBI-SRA under BioProject ID PRJNA630340.

592 **References**

593 Achkar, N. P., Cho, S. K., Poulsen, C., Arce, A. L., Re, D. A., Giudicatti, A. J., Karayekov, E., Ryu, M. Y., Choi,
594 S. W., & Harholt, J. (2018). A quick HYL1-dependent reactivation of microRNA production is
595 required for a proper developmental response after extended periods of light deprivation.
596 *Developmental cell, 46*(2), 236-247. e236.

597

598 Admoni, Y., Kozlovski, I., Lewandowska, M., & Moran, Y. (2020). TATA Binding Protein (TBP) Promoter
599 Drives Ubiquitous Expression of Marker Transgene in the Adult Sea Anemone Nematostella
600 vectensis. *Genes, 11*(9), 1081.

601
602 Alvarez-Garcia, I., & Miska, E. A. (2005). MicroRNA functions in animal development and human disease.
603 *Development, 132*(21), 4653-4662.

604
605 Axtell, M. J., Westholm, J. O., & Lai, E. C. (2011). Vive la différence: biogenesis and evolution of
606 microRNAs in plants and animals. *Genome biology, 12*(4), 1-13.

607
608 Bartel, D. P. (2004). MicroRNAs: genomics, biogenesis, mechanism, and function. *Cell, 116*(2), 281-297.

609
610 Bartel, D. P. (2018). Metazoan micrornas. *Cell, 173*(1), 20-51.

611
612 Bolger, A. M., Lohse, M., & Usadel, B. (2014). Trimmomatic: a flexible trimmer for Illumina sequence
613 data. *Bioinformatics, 30*(15), 2114-2120.

614
615 Bråte, J., Neumann, R. S., Fromm, B., Haraldsen, A. A., Tarver, J. E., Suga, H., Donoghue, P. C., Peterson,
616 K. J., Ruiz-Trillo, I., & Grini, P. E. (2018). Unicellular origin of the animal microRNA machinery.
617 *Current Biology, 28*(20), 3288-3295. e3285.

618
619 Chen, C., Ridzon, D. A., Broomer, A. J., Zhou, Z., Lee, D. H., Nguyen, J. T., Barbisin, M., Xu, N. L.,
620 Mahuvakar, V. R., & Andersen, M. R. (2005). Real-time quantification of microRNAs by stem–
621 loop RT–PCR. *Nucleic acids research, 33*(20), e179-e179.

622
623 Curtin, S. J., Watson, J. M., Smith, N. A., Eamens, A. L., Blanchard, C. L., & Waterhouse, P. M. (2008). The
624 roles of plant dsRNA-binding proteins in RNAi-like pathways. *FEBS letters, 582*(18), 2753-2760.

625
626 Dang, Y., Yang, Q., Xue, Z., & Liu, Y. (2011). RNA interference in fungi: pathways, functions, and
627 applications. *Eukaryotic cell, 10*(9), 1148-1155.

628
629 Dias, R., Manny, A., Kolaczkowski, O., & Kolaczkowski, B. (2017). Convergence of domain architecture,
630 structure, and ligand affinity in animal and plant RNA-binding proteins. *Molecular biology and*
631 *evolution, 34*(6), 1429-1444.

632
633 Dobin, A., Davis, C. A., Schlesinger, F., Drenkow, J., Zaleski, C., Jha, S., Batut, P., Chaisson, M., & Gingeras,
634 T. R. (2013). STAR: ultrafast universal RNA-seq aligner. *Bioinformatics, 29*(1), 15-21.

635

636 Dong, Z., Han, M.-H., & Fedoroff, N. (2008). The RNA-binding proteins HYL1 and SE promote accurate in
637 vitro processing of pri-miRNA by DCL1. *Proceedings of the National Academy of Sciences,*
638 *105*(29), 9970-9975.

639
640 Fridrich, A., Modepalli, V., Lewandowska, M., Aharoni, R., & Moran, Y. (2020). Unravelling the
641 developmental and functional significance of an ancient Argonaute duplication. *Nature*
642 *communications, 11*(1), 1-12.

643
644 Friedländer, M. R., Mackowiak, S. D., Li, N., Chen, W., & Rajewsky, N. (2012). miRDeep2 accurately
645 identifies known and hundreds of novel microRNA genes in seven animal clades. *Nucleic acids*
646 *research, 40*(1), 37-52.

647
648 Fukunaga, R., Han, B. W., Hung, J.-H., Xu, J., Weng, Z., & Zamore, P. D. (2012). Dicer partner proteins
649 tune the length of mature miRNAs in flies and mammals. *Cell, 151*(3), 533-546.

650
651 Genikhovich, G., & Technau, U. (2009). Induction of spawning in the starlet sea anemone Nematostella
652 vectensis, in vitro fertilization of gametes, and dejellying of zygotes. *Cold Spring Harbor*
653 *Protocols, 2009*(9), pdb. prot5281.

654
655 Han, J., Lee, Y., Yeom, K.-H., Kim, Y.-K., Jin, H., & Kim, V. N. (2004). The Drosha-DGCR8 complex in
656 primary microRNA processing. *Genes & development, 18*(24), 3016-3027.

657
658 Han, M.-H., Goud, S., Song, L., & Fedoroff, N. (2004). The Arabidopsis double-stranded RNA-binding
659 protein HYL1 plays a role in microRNA-mediated gene regulation. *Proceedings of the National*
660 *Academy of Sciences, 101*(4), 1093-1098.

661
662 He, S., Del Viso, F., Chen, C.-Y., Ikmi, A., Kroesen, A. E., & Gibson, M. C. (2018). An axial Hox code
663 controls tissue segmentation and body patterning in Nematostella vectensis. *Science, 361*(6409),
664 1377-1380.

665
666 Hutvagner, G., & Simard, M. J. (2008). Argonaute proteins: key players in RNA silencing. *Nature reviews*
667 *Molecular cell biology, 9*(1), 22-32.

668
669 Karabulut, A., He, S., Chen, C.-Y., McKinney, S. A., & Gibson, M. C. (2019). Electroporation of short
670 hairpin RNAs for rapid and efficient gene knockdown in the starlet sea anemone, Nematostella
671 vectensis. *Developmental biology, 448*(1), 7-15.

672
673 Kim, J. H., Lee, S.-R., Li, L.-H., Park, H.-J., Park, J.-H., Lee, K. Y., Kim, M.-K., Shin, B. A., & Choi, S.-Y. (2011).
674 High cleavage efficiency of a 2A peptide derived from porcine teschovirus-1 in human cell lines,
675 zebrafish and mice. *PloS one, 6*(4), e18556.

676
677 Kim, V. N., Han, J., & Siomi, M. C. (2009). Biogenesis of small RNAs in animals. *Nature reviews Molecular*
678 *cell biology, 10*(2), 126-139.

679
680 Koscianska, E., Starega-Roslan, J., & Krzyzosiak, W. J. (2011). The role of Dicer protein partners in the
681 processing of microRNA precursors. *PloS one, 6*(12).

682
683 Langmead, B., Trapnell, C., Pop, M., & Salzberg, S. L. (2009). Ultrafast and memory-efficient alignment of
684 short DNA sequences to the human genome. *Genome biology, 10*(3), 1-10.

685
686 Lee, H. Y., & Doudna, J. A. (2012). TRBP alters human precursor microRNA processing in vitro. *Rna,*
687 *18*(11).

688
689 Lewandowska, M., Sharoni, T., Admoni, Y., Aharoni, R., & Moran, Y. (2021). Functional characterization
690 of the cnidarian antiviral immune response reveals ancestral complexity. *Molecular biology and*
691 *evolution, 38*(10), 4546-4561.

692
693 Li, B., & Dewey, C. N. (2011). RSEM: accurate transcript quantification from RNA-Seq data with or
694 without a reference genome. *BMC bioinformatics, 12*(1), 1-16.

695
696 Liao, Y., Smyth, G. K., & Shi, W. (2014). featureCounts: an efficient general purpose program for
697 assigning sequence reads to genomic features. *Bioinformatics, 30*(7), 923-930.

698
699 Livak, K. J., & Schmittgen, T. D. (2001). Analysis of relative gene expression data using real-time
700 quantitative PCR and the 2− ΔΔCT method. *methods, 25*(4), 402-408.

701
702 Lorenz, R., Bernhart, S. H., Höner zu Siederdissen, C., Tafer, H., Flamm, C., Stadler, P. F., & Hofacker, I. L.
703 (2011). ViennaRNA Package 2.0. *Algorithms for molecular biology, 6*(1), 1-14.

704
705 Martin, M. (2011). Cutadapt removes adapter sequences from high-throughput sequencing reads.
706 *EMBnet. journal, 17*(1), 10-12.

707
708 Maxwell, E. K., Ryan, J. F., Schnitzler, C. E., Browne, W. E., & Baxevanis, A. D. (2012). MicroRNAs and
709 essential components of the microRNA processing machinery are not encoded in the genome of
710 the ctenophore Mnemiopsis leidyi. *BMC genomics, 13*(1), 1-11.

711
712 Modepalli, V., Fridrich, A., Agron, M., & Moran, Y. (2018). The methyltransferase HEN1 is required in
713 Nematostella vectensis for microRNA and piRNA stability as well as larval metamorphosis. *PLoS*
714 *genetics, 14*(8), e1007590.

Moran, Y., Agron, M., Praher, D., & Technau, U. (2017). The evolutionary origin of plant and animal microRNAs. *Nature ecology & evolution, 1*(3), 1-8.

Moran, Y., Fredman, D., Praher, D., Li, X. Z., Wee, L. M., Rentzsch, F., Zamore, P. D., Technau, U., & Seitz, H. (2014). Cnidarian microRNAs frequently regulate targets by cleavage. *Genome research, 24*(4), 651-663.

Moran, Y., Praher, D., Fredman, D., & Technau, U. (2013). The evolution of microRNA pathway protein components in Cnidaria. *Molecular biology and evolution, 30*(12), 2541-2552.

Pélissier, T., Clavel, M., Chaparro, C., Pouch-Pélissier, M.-N., Vaucheret, H., & Deragon, J.-M. (2011). Double-stranded RNA binding proteins DRB2 and DRB4 have an antagonistic impact on polymerase IV-dependent siRNA levels in Arabidopsis. *Rna, 17*(8), 1502-1510.

Praher, D., Zimmermann, B., Genikhovich, G., Columbus-Shenkar, Y., Modepalli, V., Aharoni, R., Moran, Y., & Technau, U. (2017). Characterization of the piRNA pathway during development of the sea anemone Nematostella vectensis. *RNA biology, 14*(12), 1727-1741.

Raja, P., Jackel, J. N., Li, S., Heard, I. M., & Bisaro, D. M. (2014). Arabidopsis double-stranded RNA binding protein DRB3 participates in methylation-mediated defense against geminiviruses. *Journal of virology, 88*(5), 2611-2622.

Redfern, A. D., Colley, S. M., Beveridge, D. J., Ikeda, N., Epis, M. R., Li, X., Foulds, C. E., Stuart, L. M., Barker, A., & Russell, V. J. (2013). RNA-induced silencing complex (RISC) Proteins PACT, TRBP, and Dicer are SRA binding nuclear receptor coregulators. *Proceedings of the National Academy of Sciences, 110*(16), 6536-6541.

Robinson, M. D., & Oshlack, A. (2010). A scaling normalization method for differential expression analysis of RNA-seq data. *Genome biology, 11*(3), 1-9.

Saito, K., Ishizuka, A., Siomi, H., & Siomi, M. C. (2005). Processing of pre-microRNAs by the Dicer-1–Loquacious complex in Drosophila cells. *PLoS biology, 3*(7).

Schauer, S. E., Jacobsen, S. E., Meinke, D. W., & Ray, A. (2002). DICER-LIKE1: blind men and elephants in Arabidopsis development. *Trends in plant science, 7*(11), 487-491.

Schmittgen, T. D., Lee, E. J., Jiang, J., Sarkar, A., Yang, L., Elton, T. S., & Chen, C. (2008). Real-time PCR quantification of precursor and mature microRNA. *methods, 44*(1), 31-38.

755 Schwaiger, M., Schönauer, A., Rendeiro, A. F., Pribitzer, C., Schauer, A., Gilles, A. F., Schinko, J. B., Renfer,
756 E., Fredman, D., & Technau, U. (2014). Evolutionary conservation of the eumetazoan gene
757 regulatory landscape. *Genome research, 24*(4), 639-650.

758

759 Shaner, N. C., Lin, M. Z., McKeown, M. R., Steinbach, P. A., Hazelwood, K. L., Davidson, M. W., & Tsien, R.
760 Y. (2008). Improving the photostability of bright monomeric orange and red fluorescent
761 proteins. *Nature methods, 5*(6), 545.

762

763 Song, L., Han, M.-H., Lesicka, J., & Fedoroff, N. (2007). Arabidopsis primary microRNA processing
764 proteins HYL1 and DCL1 define a nuclear body distinct from the Cajal body. *Proceedings of the*
765 *National Academy of Sciences, 104*(13), 5437-5442.

766

767 Stocks, M. B., Moxon, S., Mapleson, D., Woolfenden, H. C., Mohorianu, I., Folkes, L., Schwach, F.,
768 Dalmay, T., & Moulton, V. (2012). The UEA sRNA workbench: a suite of tools for analysing and
769 visualizing next generation sequencing microRNA and small RNA datasets. *Bioinformatics,*
770 *28*(15), 2059-2061.

771

772 Szarzynska, B., Sobkowiak, L., Pant, B. D., Balazadeh, S., Scheible, W.-R., Mueller-Roeber, B.,
773 Jarmolowski, A., & Szweykowska-Kulinska, Z. (2009). Gene structures and processing of
774 Arabidopsis thaliana HYL1-dependent pri-miRNAs. *Nucleic acids research, 37*(9), 3083-3093.

775

776 Tagami, Y., Motose, H., & Watanabe, Y. (2009). A dominant mutation in DCL1 suppresses the hyl1
777 mutant phenotype by promoting the processing of miRNA. *Rna, 15*(3), 450-458.

778

779 Tarver, J. E., Donoghue, P. C., & Peterson, K. J. (2012). Do miRNAs have a deep evolutionary history?
780 *Bioessays, 34*(10), 857-866.

781

782 Valli, A. A., Santos, B. A., Hnatova, S., Bassett, A. R., Molnar, A., Chung, B. Y., & Baulcombe, D. C. (2016).
783 Most microRNAs in the single-cell alga Chlamydomonas reinhardtii are produced by Dicer-like 3-
784 mediated cleavage of introns and untranslated regions of coding RNAs. *Genome research, 26*(4),
785 519-529.

786

787 Varkonyi-Gasic, E., Wu, R., Wood, M., Walton, E. F., & Hellens, R. P. (2007). Protocol: a highly sensitive
788 RT-PCR method for detection and quantification of microRNAs. *Plant methods, 3*(1), 12.

789

790 Voinnet, O. (2009). Origin, biogenesis, and activity of plant microRNAs. *Cell, 136*(4), 669-687.

791

792 Wu, F., Yu, L., Cao, W., Mao, Y., Liu, Z., & He, Y. (2007). The N-terminal double-stranded RNA binding
793 domains of Arabidopsis HYPONASTIC LEAVES1 are sufficient for pre-microRNA processing. *The*
794 *Plant Cell, 19*(3), 914-925.

795
796 Yamasaki, T., Onishi, M., Kim, E.-J., Cerutti, H., & Ohama, T. (2016). RNA-binding protein DUS16 plays an
797 essential role in primary miRNA processing in the unicellular alga Chlamydomonas reinhardtii.
798 *Proceedings of the National Academy of Sciences, 113*(38), 10720-10725.

799
800 Zhong, J., Peters, A. H., Lee, K., & Braun, R. E. (1999). A double-stranded RNA binding protein required
801 for activation of repressed messages in mammalian germ cells. *Nature genetics, 22*(2), 171-174.

802

803

804

805

806

807

808

809

810

811

812

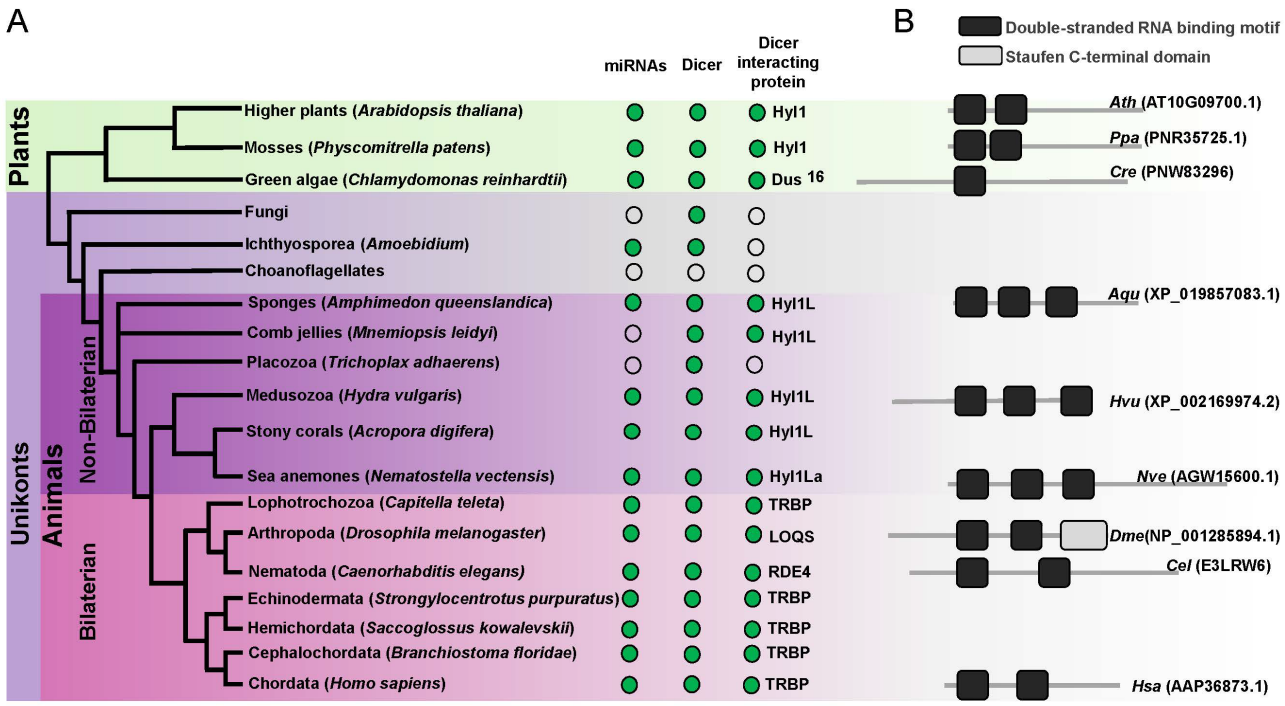

Figure 1. Schematic representation of a phylogenetic tree of Eukaryotes at the phylum level

(A) Phylogenetic tree representing the presence (green circles) and absence (open circles) of miRNAs, Dicer and Dicer interacting proteins in different plant and animal phyla. The names of representatives of different phyla are given in brackets. The names of Dicer interacting proteins are given near the green circles.

(B) Domain structure of different Dicer interacting proteins predicted by using the Pfam (https://pfam.xfam.org/). NCBI gene ID is shown in brackets.

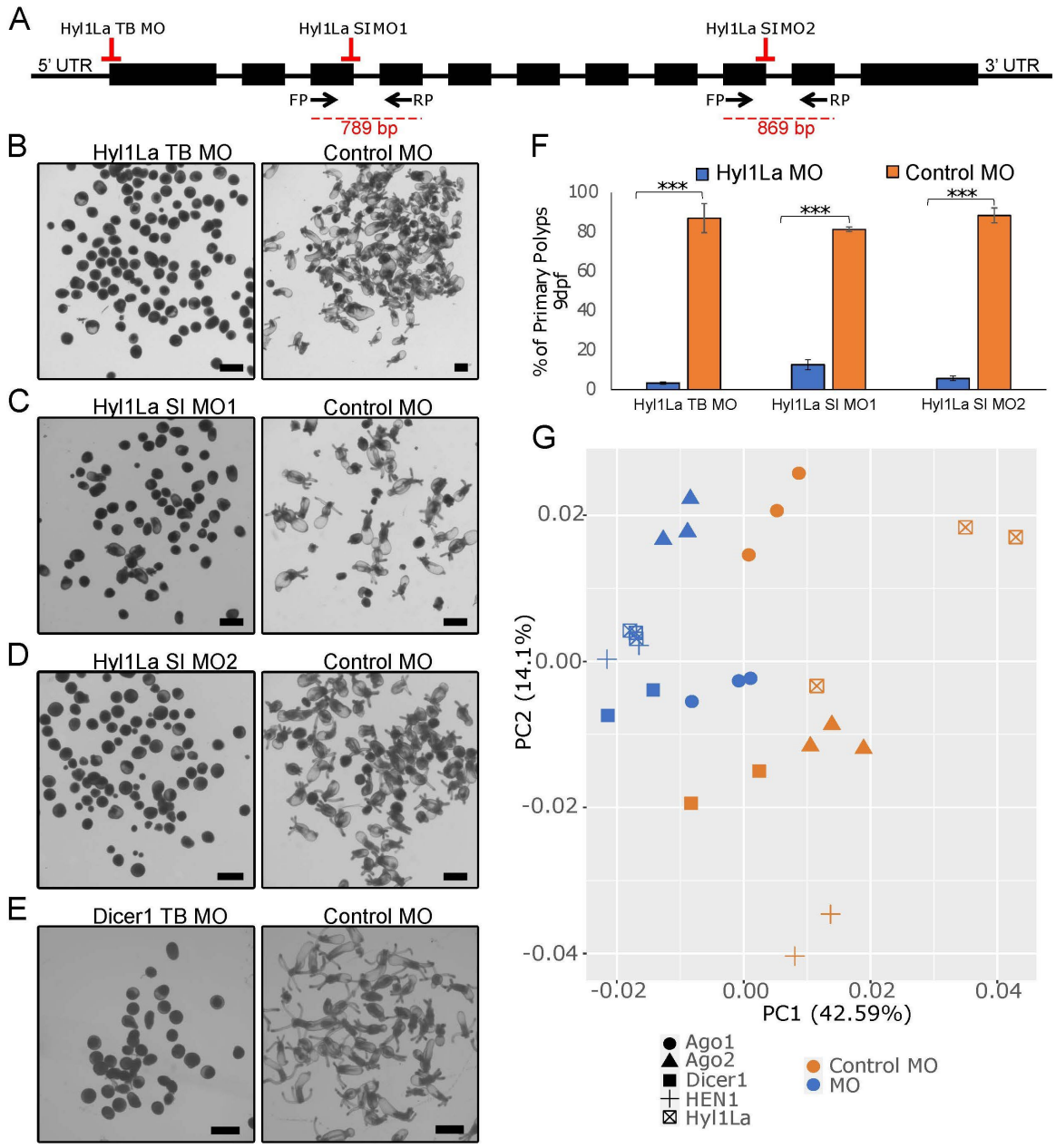

Figure 2. Developmental defects in different morphants of Hyl1La

(A) Schematic representation of the Hyl1La gene showing the intron-exon junction as defined by comparing the transcript (NCBI Accession KF192067.1) to the *Nematostella vectensis* genome. The positions targeted by different morpholinos used in the study are shown by red symbols. The black arrows represent the position of primers designed for the validation of splicing morpholino.

(B-D) Images of 9 dpf animals showing similar developmental defects in different morphants.

829 (E) Images of 10 dpf Dicer1 morphants showing similar developmental defects to Hyl1La morphants.
830 Scale bars are 500 µm.

831 (F) Bar chart representing percentage of developed and undeveloped animals for each of the morphants.
832 More than 80% of Hyl1La depleted animals did not develop into the primary polyp stage after 9 dpf. Data
833 was taken in triplicates, in each n=200, ***P<0.001 (Student's t-test).

834 (G) Principal component analysis (PCA) plot of the miRNA expression following the knockdown of
835 miRNA biogenesis components: Hyl1La, HEN1, Dicer2, AGO1 and AGO2. Morphants are in blue and
836 control in orange, different symbols represent different miRNA biogenesis components and their
837 respective controls from the same experiment.

838

839

840

841

842

843

844

845

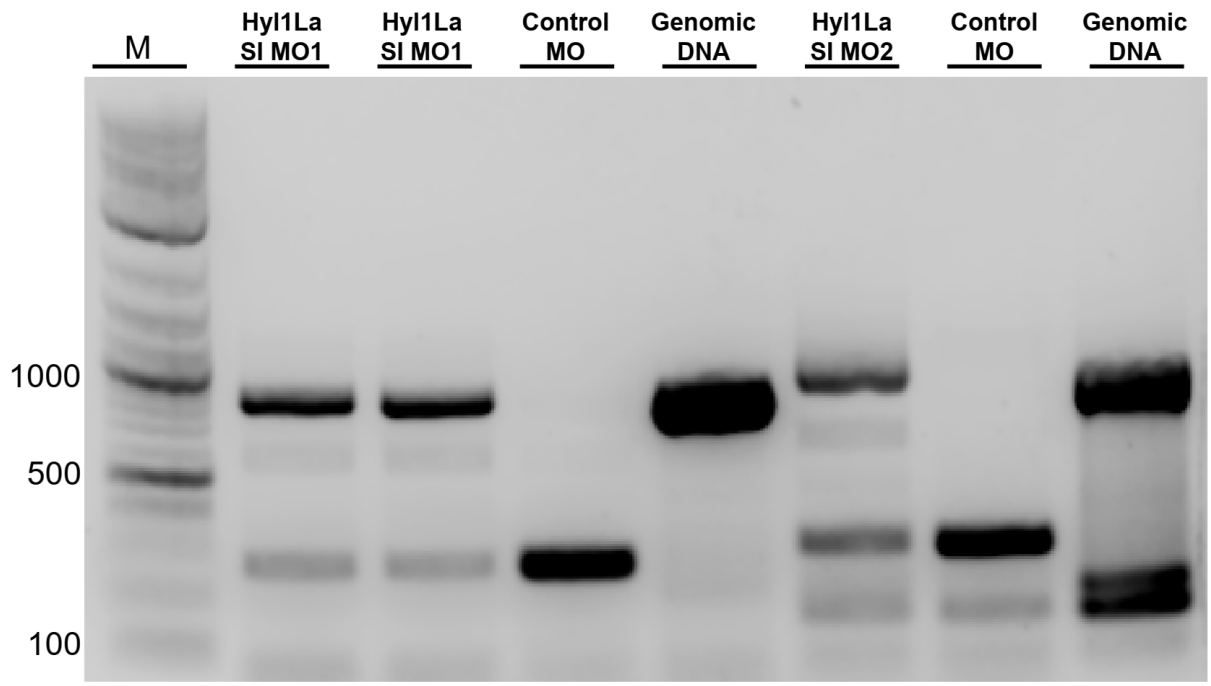

846

847

848 **Figure 2 - figure supplement 1. Gel image showing aberrant splicing of Hyl1La.** cDNAs were
849 amplified by using two different primer sets for different morpholinos (Hy1La SI MO1 and Hyl1La SI
850 MO2). The control morpholino lane showed the band of spliced Hyl1La while the Hyl1La SI morpholino
851 lane showed the band of size equivalent for intron retention. The genomic DNA was amplified by using
852 the same primer pairs to check the size and primer efficiency (Figure 2 – source data 1).

853

854

855

856

857

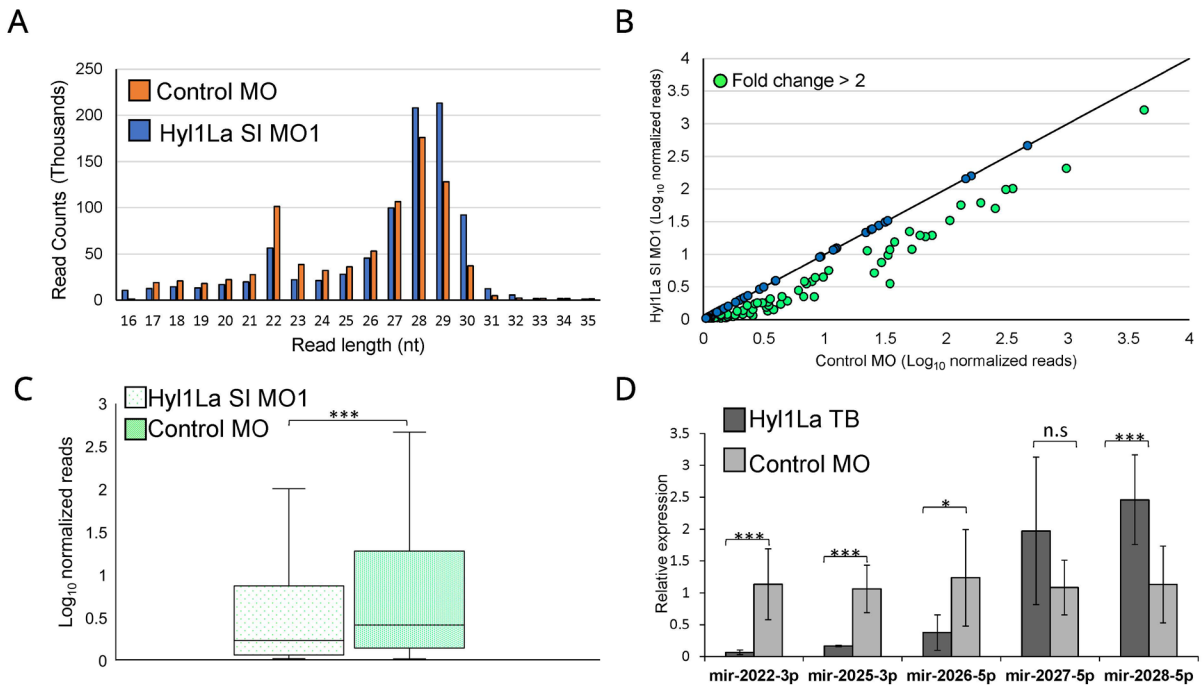

Figure 3. Hyl1La morphants show reduced expression of miRNAs

(A) Average read length distribution of small RNA reads after adapter removal.

(B) Scatter plot representing normalized read counts of miRNAs in control and treated animals. Each dot represents the average expression of an individual miRNA. The miRNAs showing a depletion greater than two-fold are indicated in green. The axes are scaled to Log_{10} of normalized read counts. The data represents the mean of three independent biological replicates.

(C) Box plot showing the average of abundance of miRNA read counts in Hyl1La SI MO1 and control MO. A significant reduction of miRNA read counts is noted in Hyl1La SI MO1, ($P < 0.0001$, Wilcoxon signed-rank test). The data represents the mean of three independent biological replicates ± SD.

(D) Bar plot showing the expression of miR-2022, miR-2025, miR-2026, miR-2027 and miR-2028 as quantified using stem-loop PCR in translation blocking (TB) and control morpholino. The data represents the mean of three independent biological replicates ± SD. ***$P< 0.001$, ** $P \leq 0.01$. * $P \leq 0.05$, (Student's t-test), n.s (not significant).

874

875

876

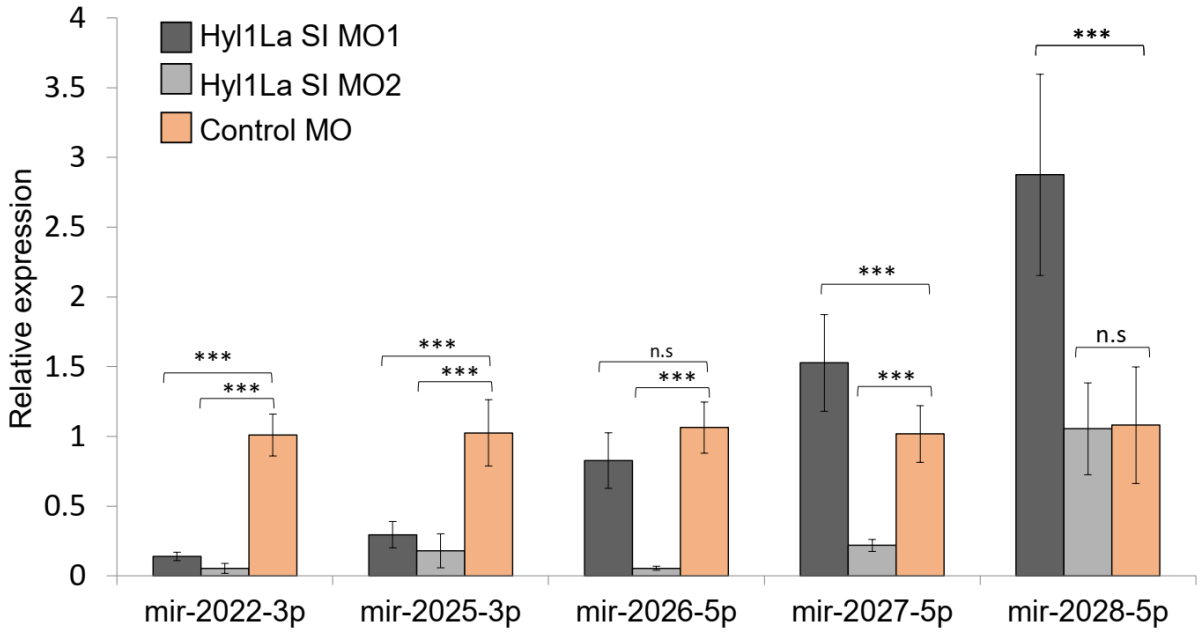

877

878

879 **Figure 3 - figure supplement 1. Effect of Hyl1La depletion on miRNA expression.**

880 The expression of miR-2022, miR-2025, miR-2026, miR-2027 and miR-2028 was checked by using the
881 stem-loop PCR between the Hyl1La SI MO1 vs. Control MO and Hyl1La SI MO2 vs. Control MO. The
882 data represents the mean of four independent biological replicates ± SD. ***P<0.001, ** P ≤ 0.01. * P ≤
883 0.05, (Student's t-test), n.s (not significant).

884

885

886

887

888

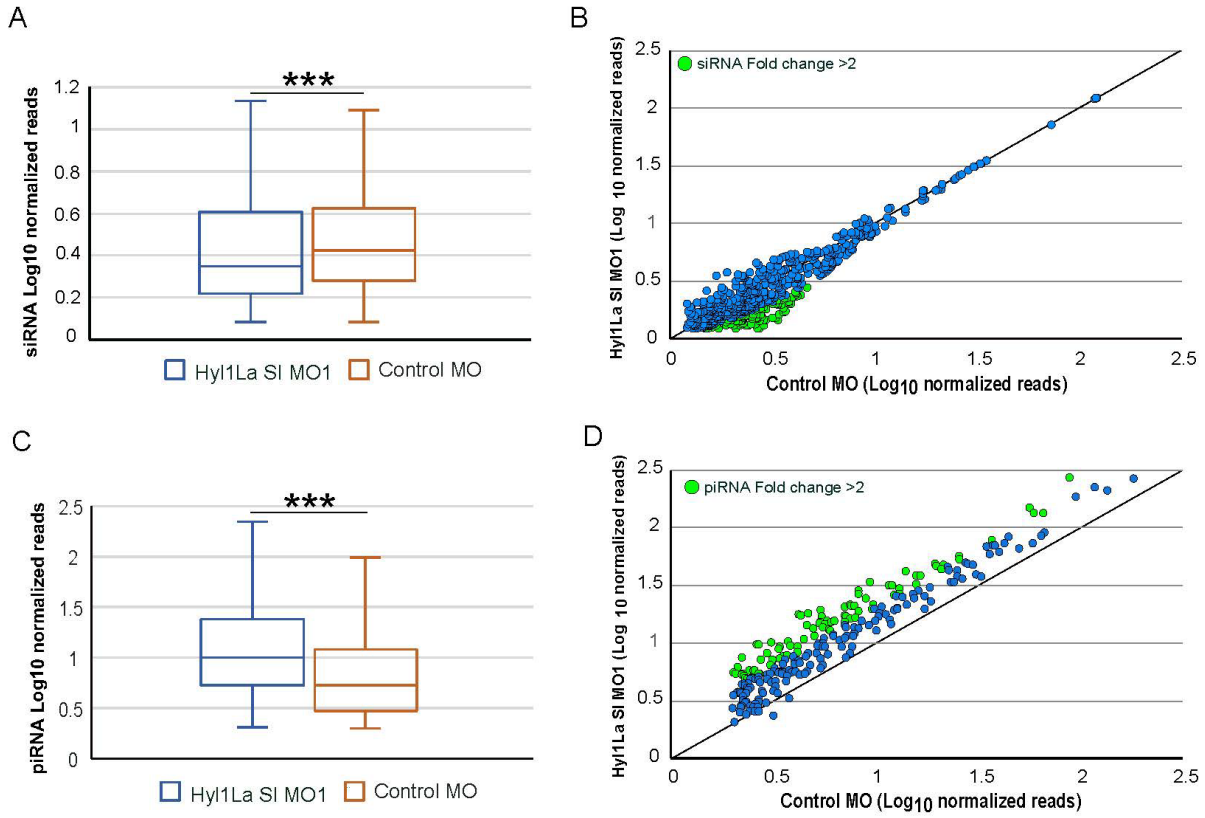

Figure 3 - figure supplement 2. Effect of Hyl1La depletion on siRNA and piRNA expression.

(A) Box plot showing the average of abundance of siRNA read counts in Hyl1La SI MO1 and control MO. A significant slight reduction of siRNA read counts is noted in Hyl1La SI MO1, ($P < 0.00001$, Wilcoxon signed-rank test). The data represents the mean of three independent biological replicates ± SD.

(B) Scatter plot representing normalized read counts of siRNAs in control and treated animals. Each dot represents the average expression of an individual siRNA. The siRNAs showing a depletion greater than two-fold are indicated in green. The axes are scaled to Log_{10} of normalized read counts. The data represents the mean of three independent biological replicates.

(C) Box plot showing the average of abundance of piRNA read counts in Hyl1La SI MO1 and control MO. A significant upregulation of piRNA read counts is noted in Hyl1La SI MO1, ($P < 0.00001$, Wilcoxon signed-rank test). The data represents the mean of three independent biological replicates ± SD.

(D) Scatter plot representing normalized read counts of piRNAs in control and treated animals. Each dot represents the average expression of an individual piRNA. The piRNAs showing an upregulation greater than two-fold are indicated in green. The axes are scaled to Log_{10} of normalized read counts. The data represents the mean of three independent biological replicates.

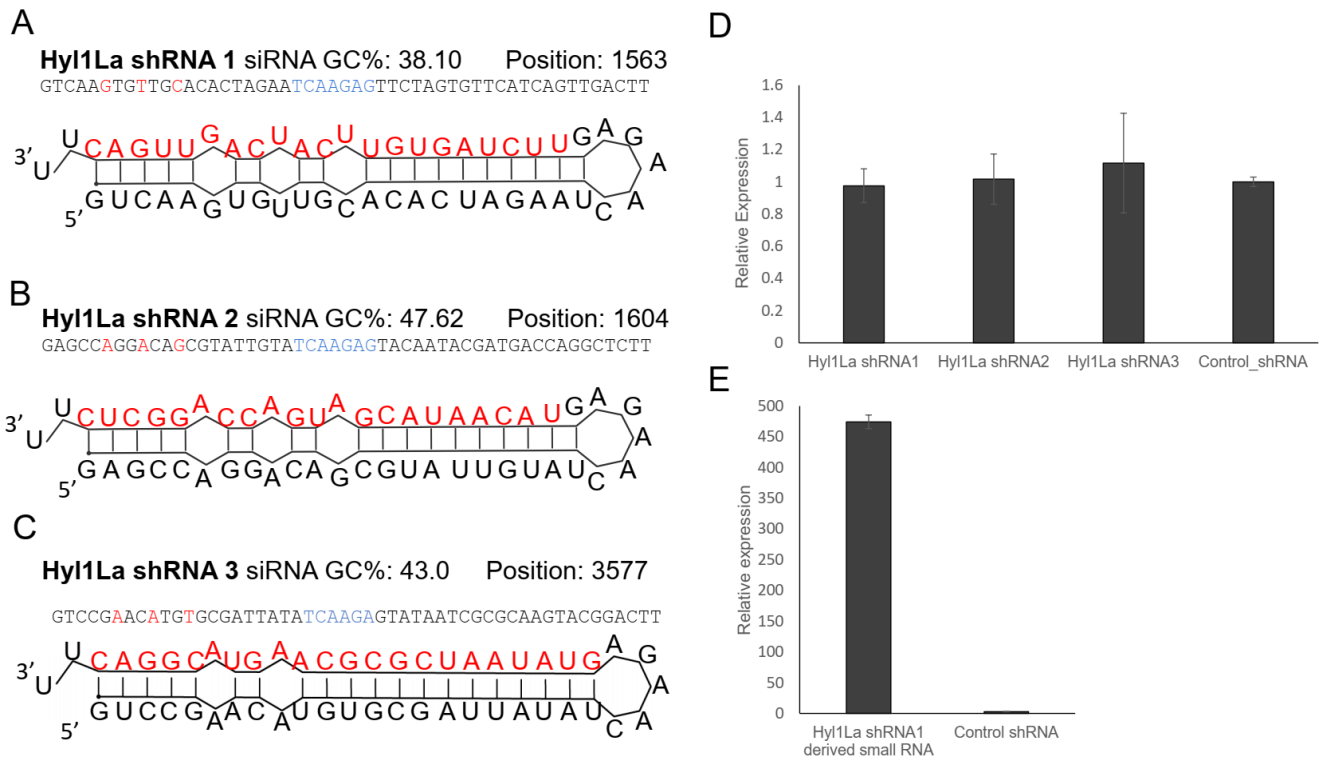

Figure 4. Structure of shRNA precursors and their effect on Hyl1La expression

(A-C) Structure of different shRNAs designed from different positions of Hyl1La gene along with GC content and their position are shown. In the shRNA sequence, the red color shows the nucleotides edited for mismatch and blue color represents loop region. The red colored nucleotides on precursor's structure indicate the small RNA derived from the shRNAs.

(D) Real time quantification of Hyl1La from animals injected with different shRNAs relative to control. The data represents the mean of three independent biological replicates ± SD.

(E) Quantification of small RNAs produced from Hyl1La shRNA1. The quantification was performed by using stem-loop qRT-PCR.

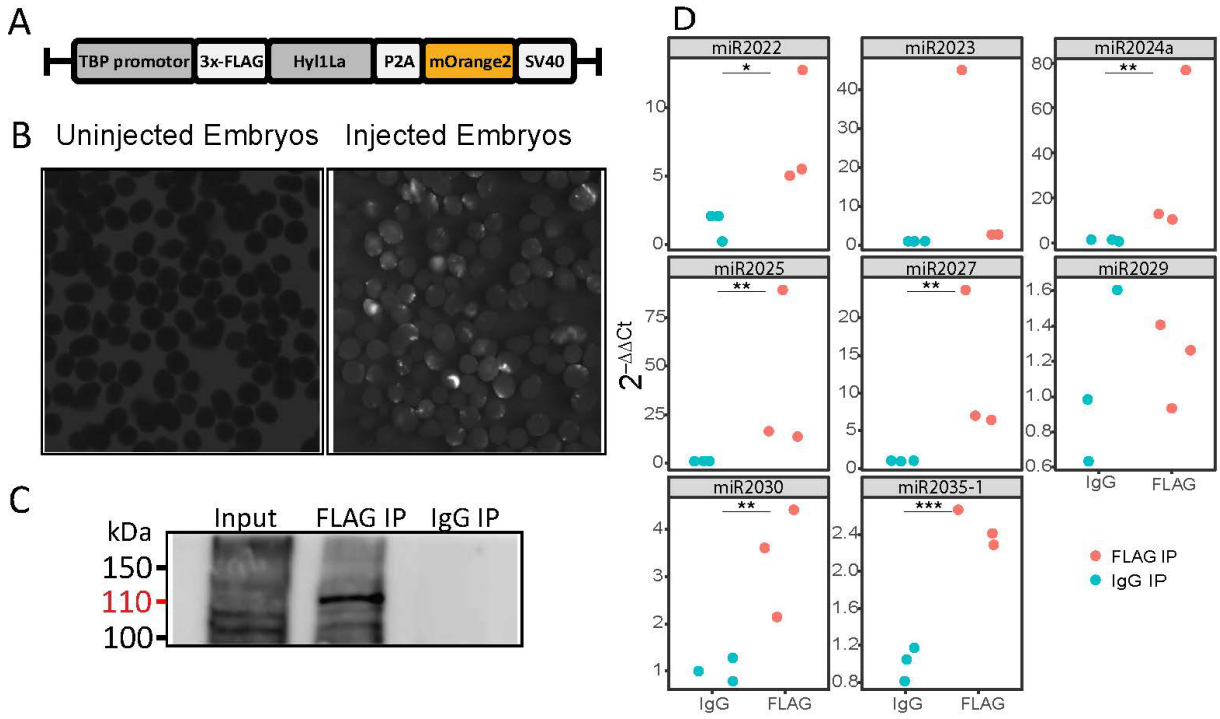

Figure 5. RNA Immunoprecipitation (RIP) and qRT-PCR

(A) Schematic representation of the FLAG-Hyl1La construct with a TBP promoter, a self-cleaving P2A sequence, a memOrange2 gene and the polyadenylation signal SV40.

(B) The plasmid-injected and uninjected embryos were visualized under a florescence microscope after two days. The injected embryos were showing the expression of memOrange2 (right side).

(C) Immunoprecipitation of 3×FLAG-Hyl1La with mouse anti-FLAG antibody or whole mouse IgG by using Protein G Magnetic Beads. The input and IP samples were subjected to Western blot with mouse anti-FLAG antibody. The red arrow (110 kDa) indicates the 3×FLAG-Hyl1La (Figure 5 - source data 3 and 4).

(D) pre-miRNA expression of eight different miRNAs were measured using the qRT-PCR. The Y-axis represents the $2^{-\Delta\Delta Ct}$ values of three independent biological replicates. ***P<0.001, **P ≤ 0.01. *P ≤ 0.05, (Student's t-test).

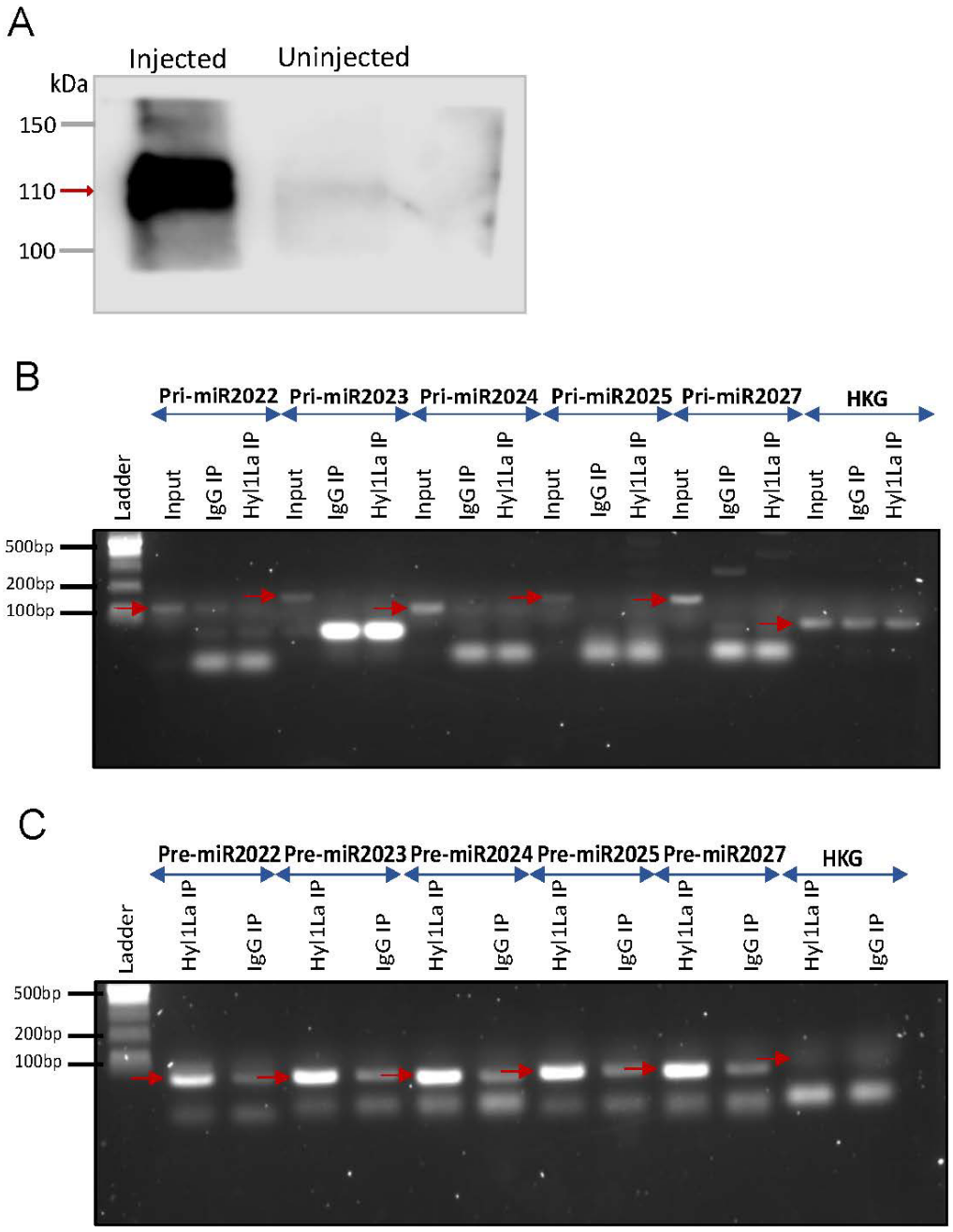

Figure 5 - figure supplement 1. RNA Immunoprecipitation (RIP) and PCR (Related to Figure 5B-D)

(A) Western blot of 3×FLAG-Hyl1La with mouse anti-FLAG antibody. (Figure 5 - source data 1 and 2) Gel image showing RT-PCR amplified (B) pri-miRNA (primary miRNA) and (C) pre-miRNA (precursor miRNA) transcripts. The pri- and pre-miRNA were amplified with their specific primers from RNA isolated from samples immunoprecipitated with mouse anti-FLAG antibody (Hyl1La IP)/whole mouse IgG (IgG IP). The red arrow indicates the expected product size. Ubiquitin was taken as control housekeeping gene (HKG). (Figure 5 - source data 5 and 6)

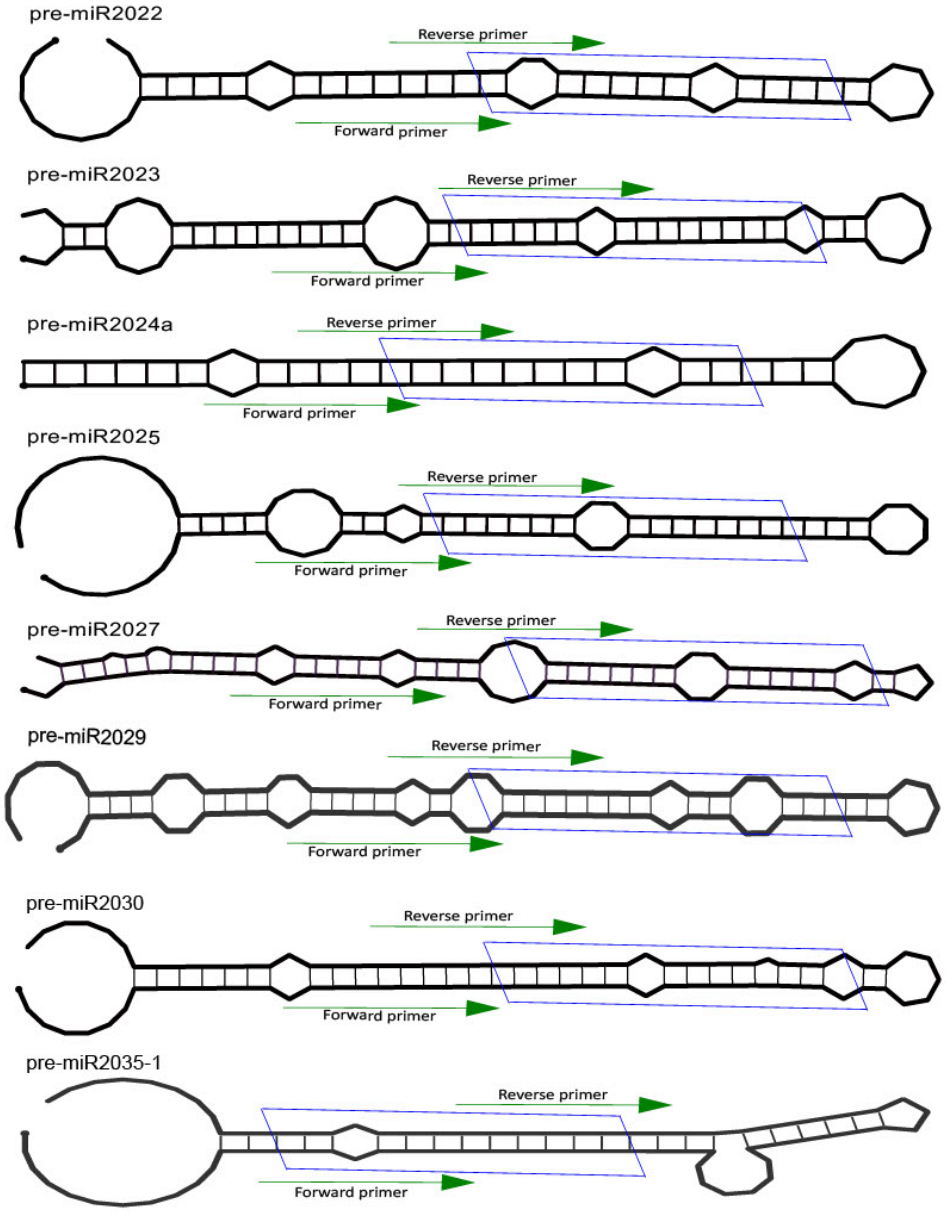

Figure 5 - figure supplement 2. Position of primers on pre-miRNA

The secondary structure of miRNA precursors used in this study for identification of functional interaction with Hyl1La. The green arrow indicates the primer positions used for pre-miRNA quantification. The blue box represents position of miRNA/miRNA* duplex.

>nve-mir-2022
AGCGTGGGGATGCAGACAGATAATCTCGGGATGAGTTCGCCTGAATGATCAAGATGAGTTC
GCCTGAAAGTCGGGATGAGATCGCCTGAGAGTCGGGATAAGATCGCCTGAAAGTCGGGATA
AATCAACTGTCAAGTGGTTGTCATTTGCTAGTTGCTTTTGTCCCGCCTTTTCTGCGAATTGAT
CACGTGATGTGACGTCATCACTGCCCAATTACAAATGCTGCAATATATTGAGGTACGTAAAC
GTTAGATGTTGCGCATATACCTCATACG

>nve-mir-2023
GACTAGCTCAGTGGATCGACTAATTGGGGAATGGGCTATAGAAGACGACGATTACTATCAA
AATAGCTCAGTGGGCCAAGTACTGGAGACCAGACGAGAAGAGTTGCGTGACATACCTGTGT
CTGCCACCTGTATTTCTATCACGTCAGATGAAAGAAGTACAAGTGGTAGGGAAGGGTGTGTC
GATTGACAATGGCGGCTTATCAAGACACGACCAATGTTGTAAGGGAGGAGGTAGATATACA
AGAATGCAGCAGAAATAGTTTACAAGCTTCGAGGTAAGGGAGGGAGTA

>nve-mir-2024a

CAAGAGCGATCGAGCACACGTGAGTCAGAATATTGCTTATGTTCTATAAGTATTCCTGGTAA
TTTTGAGGAGGCGATGTAACTCTACCAACAAGTGCTACTGCTTCAAAATATCGGTGTTGGGT
AAAAGGTCACATT**TTACACAGTACCGATATTGTGA**AGCACGTTTGCTTAGGAACTAGGATA
CAACGAGGAGGCAAATTAAAGCTACCAACAAGCGCTGTAACTCCACACGAAGACAGGTAAC
GAGAGAAATCAAGCCCG

>nve-mir-2025
GTAAAAGCATGTATGTGTTTTAACGCTAGTGCAGTAGCAAAACTACAACCGGGAGTGGAGA
CCCAAAAGGCGTTCATGTCGACACAGCAAGAATATGATCAACAATTAGGCCACATACAAAG
CTTTCGATGGCTAGAAAATCCTTAGTGATTTTTTAGCCCGCGGAAGTTGTGTTGCCTGGCCAA
TATTACCATTAGGGTGAAGGCAATGATCAAGACGAGGTTGTACTGGAAGACGCGAAGGCTG
TTTATTTATATTACAGTATAAGGGTAAGAAACATCGGTTACTTTGAAGG

>nve-mir-2027
CCTTGGAATCTCTCAGCTTCAAGAGCAGCAGCAAGCCCCTAGTAATTGATGTATTCAGTTTG
TTTTCAAACAAGATAGAGCTGCACACCTCAGATCTTTCAATCCGAGAGCCTTAAGGCTT**GCT**
TGTTGGTAATTTTGCATCTGTTGCACATGCGATTTTACCAAAATGCAATTCTTATGGTTCAG
TGATCAGGAACCCAATAACTGCAGCACAGTTGTCTGATATCGGTGCATGAAACTGATAGTCA
CTACAGTTTTTAAATTCATCTAATATAATAACTTCCAAGGGCTTATTT

Figure 5 - figure supplement 3. Position of pre- and pri-miRNA primers on probable sequence of pri-miRNA

The probable sequence of pri-miRNA taken from the *Nematostella* genome browser (https://simrbase.stowers.org/). The underlined sequences represent the pre-miRNA. The sequences with purple and green color represents primer position for pri- and pre-miRNA, respectively.

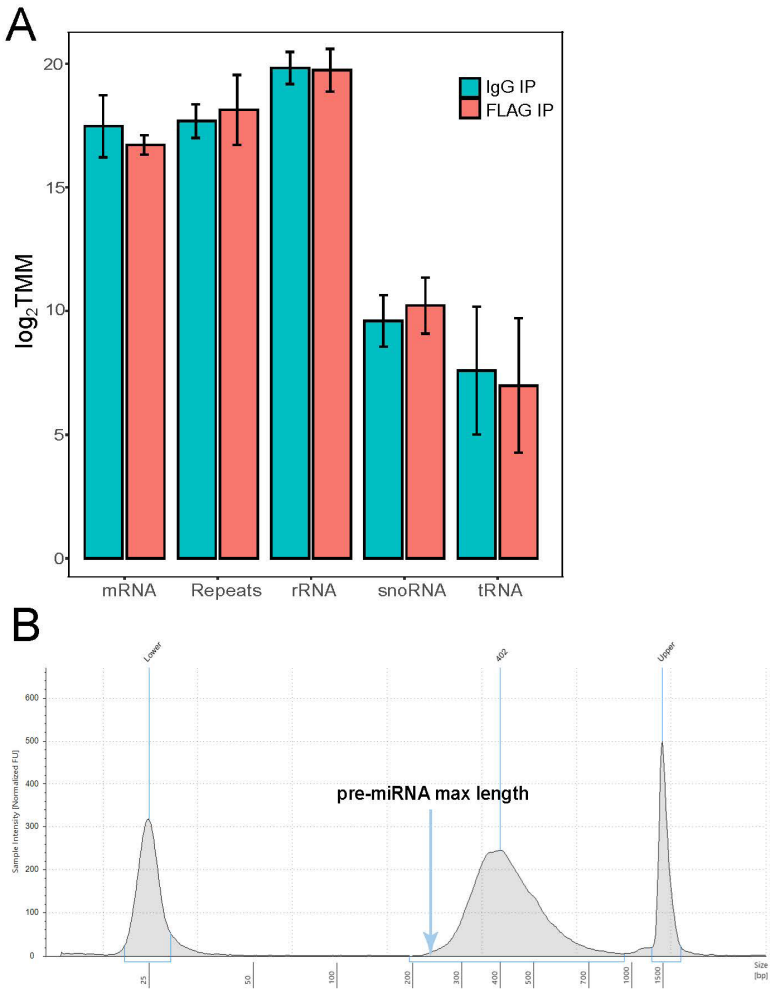

989

990 **Figure 5 - figure supplement 4. RNA-seq of RNA Immunoprecipitation (RIP)**

991 (A) Immunoprecipitation RNA sequencing of FLAG-Hyl1La. Read-counts mapped to the *Nematostella*
992 genome were log2 and trimmed mean of m (TMM) normalized. A combination of coding (mRNA), non-
993 coding RNA (rRNA, snoRNA, tRNA) and repetitive elements were quantified for both FLAG-Hyl1La
994 and IgG. Error bars correspond to standard deviation among replicates (n=4). All comparisons were not
995 significant (Student's t-test).

996 (B) Representation of size distribution of libraries generated from RIP samples, validated with
997 TapeStation system (Agilent, USA).

998

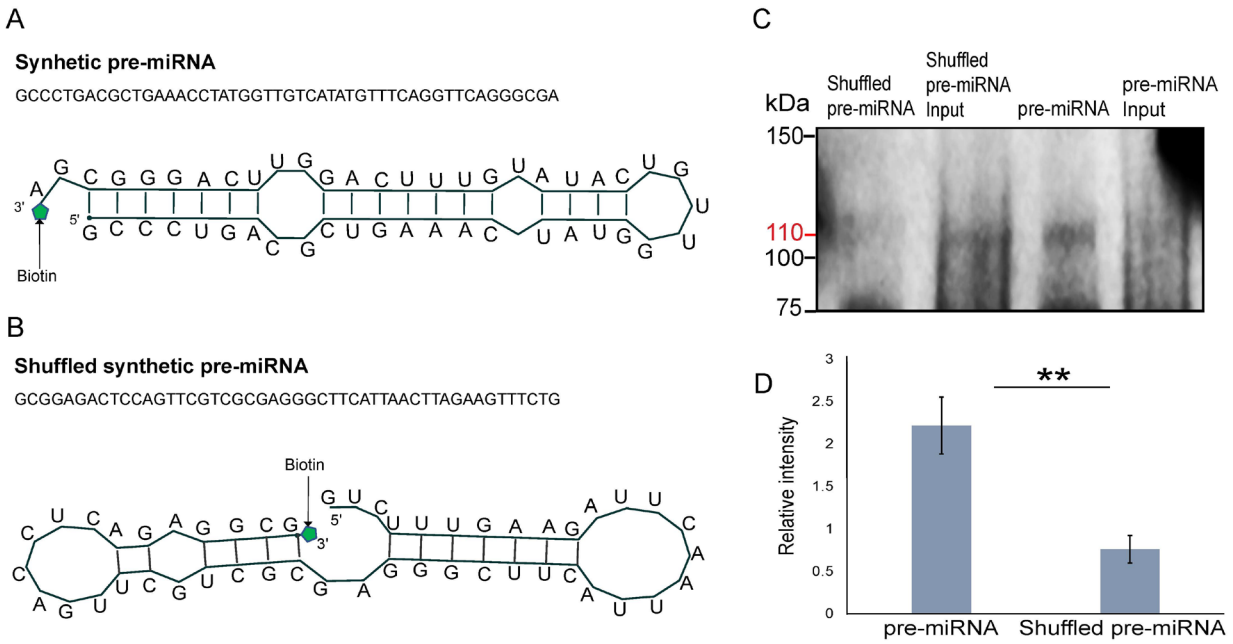

Figure 6 – In vitro binding assay

(A) The sequence and secondary structure of biotin-labeled synthetic pre-miRNA used for in vitro binding assay.

(B) The sequence and secondary structure of biotin-labeled shuffled synthetic pre-miRNA used as negative control for in vitro binding assay.

(C) Pull-down of biotin labeled synthetic pre-miRNA and shuffled pre-miRNA negative control using streptavidin magnetic beads. The pull-down samples were subjected to Western blot with mouse anti-FLAG antibody (Figure 6 – source data 1-6).

(D) Relative intensity of Western blot bands with mouse anti-FLAG antibody, showing pull-down of biotin labeled synthetic pre-miRNA and shuffled pre-miRNA negative control. Error bars correspond to standard deviation among replicates (n=3). **$P \leq 0.01$ (Student's t-test).